of two types of microarray, BAC array and oligonucleotide array. The BAC array was applied for 298 patients to detect 58 CNVs in 47 patients, and among them 26 CNVs (8.7%) were determined to be causal (pathogenic). Conversely, the oligonucleotide arrays were applied for 703 patients to detect 1538 CNVs in 603 patients, and among them 74 CNVs (10.5%) were determined to be pathogenic. These results may lead to the following idea: a lower-resolution microarray detects a limited number of CNVs likely to be pathogenic, because such CNVs tend to be large, and a higher-resolution microarray detects an increasing number of bCNVs or VOUS.[38] Indeed, in studies using a high-resolution microarray, most of the CNVs detected were smaller than 500 kb but almost all pCNVs were relatively large.[54,81,83] Most of the small CNVs were judged not to be pathogenic, and the percentage of pCNVs stabilized at around 10%. This percentage may suggest a frequency of patients with MCA/MR caused by CNV affecting one or more genes, other than known syndromes and subtelomeric aberrations. The other patients may be affected by another cause undetectable by genomic microarray; for example a point mutation or microdeletion/duplication of a single gene, aberration of microRNA, aberration of methylation states, epigenetic aberration or partial uniparental disomy.

As recently hypothesized secondary insult, which is potentially another CNV, a mutation in a phenotypically related gene or an environmental event influencing the phenotype, may result in clinical manifestation.[84] Especially, in two-hit CNVs, two models have been hypothesized: (1) the additive model of two co-occurring CNVs affecting independent functional modules and (2) the epistatic model of two CNVs affecting the same functional module.[85] It also suggests difficulty in selecting an optimal platform in the clinical screening. Nevertheless, information on both pCNVs and bCNVs detected through studies using several types of microarrays is unambiguously significant because an accumulation of the CNVs will create a map of genotype–phenotype correlation that would determine the clinical significance of each CNV, illuminate gene function or establish a new syndrome.

ACKNOWLEDGEMENTS

We thank Ayako Takahashi and Rumi Mori for technical assistance. This study was supported by the Joint Usage/Research Program of Medical Research Institute, Tokyo Medical and Dental University. This work was also supported by grants-in-aid for Scientific Research on Priority Areas from the Ministry of Education, Culture, Sports, Science, and Technology, Japan; a grant from Core Research for Evolutional Science and Technology (CREST) of the Japan Science and Technology Corporation (JST); a grant from the New Energy and Industrial Technology Development Organization (NEDO); and in part by Grant-in-Aid for Scientific Research (B) (17390099, 20390301) of Japan Society for the Promotion of Science (JSPS); Health and Labour Sciences Research Grants for Research on information system of undiagnosed diseases (H21-nanchi-ippan-167) and Research on policy for intractable diseases (H22-nanchi-shitei-001) from the Ministry of Health, Labour and Welfare, Japan.

1 Roeleveld, N., Zielhuis, G. A. & Gabreëls, F. The prevalence of mental retardation: a critical review of recent literature. *Dev. Med. Child Neurol.* **39,** 125–132 (1997).
2 Hunter, A. G. Outcome of the routine assessment of patients with mental retardation in a genetics clinic. *Am. J. Med. Genet.* **90,** 60–68 (2000).
3 Smith, D. W. & Bostian, K. E. Congenital anomalies associated with idiopathic mental retardation. *J. Pediatr.* **65,** 189–196 (1964).
4 Gustavson, K. H., Hagberg, B., Hagberg, G. & Sars, K. Severe mental retardation in a Swedish county. II. Etiologic and pathogenetic aspects of children born 1959–1970. *Neuropadiatrie* **8,** 293–304 (1977).
5 Fryns, J. P., Kleczkowska, A., Kubień, E. & Van den Berghe, H. Cytogenetic findings in moderate and severe mental retardation. A study of an institutionalized population of 1991 patients. *Acta. Paediatr. Scand. Suppl.* **313,** 1–23 (1984).
6 Gustavson, K. H., Holmgren, G. & Blomquist, H. K. Chromosomal aberrations in mildly mentally retarded children in a northern Swedish county. *Ups. J. Med. Sci. Suppl.* **44,** 165–168 (1987).
7 Schreppers-Tijdink, G. A., Curfs, L. M., Wiegers, A., Kleczkowska, A. & Fryns, J. P. A systematic cytogenetic study of a population of 1170 mentally retarded and/or behaviourly disturbed patients including fragile X-screening. The Hondsberg experience. *J. Genet Hum.* **36,** 425–446 (1988).
8 van Karnebeek, C. D., Koevoets, C., Sluijter, S., Bijlsma, E. K., Smeets, D. F., Redeker, E. J. *et al.* Prospective screening for subtelomeric rearrangements in children with mental retardation of unknown aetiology: the Amsterdam experience. *J. Med. Genet.* **39,** 546–553 (2002).
9 Vissers, L. E., de Vries, B. B., Osoegawa, K., Janssen, I. M., Feuth, T., Choy, C. O. *et al.* Array-based comparative genomic hybridization for the genomewide detection of submicroscopic chromosomal abnormalities. *Am. J. Hum. Genet.* **73,** 1261–1270 (2003).
10 Pickering, D. L., Eudy, J. D., Olney, A. H., Dave, B. J., Golden, D., Stevens, J. *et al.* Array-based comparative genomic hybridization analysis of 1176 consecutive clinical genetics investigations. *Genet. Med.* **10,** 262–266 (2008).
11 Bauters, M., Van Esch, H., Marynen, P. & Froyen, G. X chromosome array-CGH for the identification of novel X-linked mental retardation genes. *Eur. J. Med. Genet.* **48,** 263–275 (2005).
12 Hayashi, S., Honda, S., Minaguchi, M., Makita, Y., Okamoto, N., Kosaki, R. *et al.* Construction of a high-density and high-resolution human chromosome X array for comparative genomic hybridization analysis. *J. Hum. Genet.* **52,** 397–405 (2007).
13 Kok, K., Dijkhuizen, T., Swart, Y. E., Zorgdrager, H., van der Vlies, P., Fehrmann, R. *et al.* Application of a comprehensive subtelomere array in clinical diagnosis of mental retardation. *Eur. J. Med. Genet.* **48,** 250–262 (2005).
14 Friedman, J. M., Baross, A., Delaney, A. D., Ally, A., Arbour, L., Armstrong, L. *et al.* Oligonucleotide microarray analysis of genomic imbalance in children with mental retardation. *Am. J. Hum. Genet.* **79,** 500–513 (2006).
15 Xiang, B., Li, A., Valentin, D., Nowak, N. J., Zhao, H. & Li, P. Analytical and clinical validity of whole-genome oligonucleotide array comparative genomic hybridization for pediatric patients with mental retardation and developmental delay. *Am. J. Med. Genet.* **146A,** 1942–1954 (2008).
16 Shen, Y., Irons, M., Miller, D. T., Cheung, S. W., Lip, V., Sheng, X. *et al.* Development of a focused oligonucleotide-array comparative genomic hybridization chip for clinical diagnosis of genomic imbalance. *Clin. Chem.* **53,** 2051–2059 (2007).
17 McMullan, D. J., Bonin, M., Hehir-Kwa, J. Y., de Vries, B. B., Dufke, A., Rattenberry, E. *et al.* Molecular karyotyping of patients with unexplained mental retardation by SNP arrays: a multicenter study. *Hum. Mutat.* **30,** 1082–1092 (2009).
18 Iafrate, A. J., Feuk, L., Rivera, M. N., Listewnik, M. L., Donahoe, P. K., Qi, Y. *et al.* Detection of large-scale variation in the human genome. *Nat. Genet.* **36,** 949–951 (2004).
19 Sebat, J., Lakshmi, B., Troge, J., Alexander, J., Young, J., Lundin, P. *et al.* Large-scale copy number polymorphism in the human genome. *Science.* **305,** 525–528 (2004).
20 Redon, R., Ishikawa, S., Fitch, K. R., Feuk, L., Perry, G. H., Andrews, T. D. *et al.* Global variation in copy number in the human genome. *Nature* **444,** 444–454 (2006).
21 Lee, C., Iafrate, A. J. & Brothman, A. R. Copy number variations and clinical cytogenetic diagnosis of constitutional disorders. *Nat. Genet.* **39,** S48–S54 (2007).
22 Inazawa, J., Inoue, J. & Imoto, I. Comparative genomic hybridization (CGH)-arrays pave the way for identification of novel cancer-related genes. *Cancer Sci.* **95,** 559–563 (2004).
23 Hayashi, S., Kurosawa, K., Imoto, I., Mizutani, S. & Inazawa, J. Detection of cryptic chromosome aberrations in a patient with a balanced t(1;9)(p34.2;p24) by array-based comparative genomic hybridization. *Am. J. Med. Genet.* **139,** 32–36 (2005).
24 Shrimpton, A. E., Braddock, B. R., Thomson, L. L., Stein, C. K. & Hoo, J. J. Molecular delineation of deletions on 2q37.3 in three cases with an Albright hereditary osteodystrophy-like phenotype. *Clin. Genet.* **66,** 537–544 (2004).
25 Rauch, A. & Dörr, H. G. Chromosome 5q subtelomeric deletion syndrome. *Am. J. Med. Genet. C* **145C,** 372–376 (2007).
26 Horn, D., Tönnies, H., Neitzel, H., Wahl, D., Hinkel, G. K., von Moers, A. *et al.* Minimal clinical expression of the holoprosencephaly spectrum and of Currarino syndrome due to different cytogenetic rearrangements deleting the Sonic Hedgehog gene and the HLXB9 gene at 7q36.3. *Am. J. Med. Genet. A* **128A,** 85–92 (2004).
27 Tatton-Brown, K., Pilz, D. T., Orstavik, K. H., Patton, M., Barber, J. C., Collinson, M. N. *et al.* 15q overgrowth syndrome: a newly recognized phenotype associated with overgrowth, learning difficulties, characteristic facial appearance, renal anomalies and increased dosage of distal chromosome 15q. *Am. J. Med. Genet. A* **149A,** 147–154 (2009).
28 Lu, X., Shaw, C. A., Patel, A., Li, J., Cooper, M. L., Wells, W. R. *et al.* Clinical implementation of chromosomal microarray analysis: summary of 2513 postnatal cases. *PLoS One* **2,** e327 (2007).
29 Fernandez, T. V., García-González, I. J., Mason, C. E., Hernández-Zaragoza, G., Ledezma-Rodríguez, V. C., Anguiano-Alvarez, V. M. *et al.* Molecular characterization of a patient with 3p deletion syndrome and a review of the literature. *Am. J. Med. Genet. A* **146A,** 2746–2752 (2008).
30 Jones, K. L. *Smith's Recognizable Patterns of Human Malformation,* 6th edn. (Elsevier Saunders, Philadelphia, 2006).
31 Striano, P., Malacarne, M., Cavani, S., Pierluigi, M., Rinaldi, R., Cavaliere, M. L. *et al.* Clinical phenotype and molecular characterization of 6q terminal deletion syndrome: five new cases. *Am. J. Med. Genet. A* **140,** 1944–1949 (2006).

32 Lindstrand, A., Malmgren, H., Verri, A., Benetti, E., Eriksson, M., Nordgren, A. *et al.* Molecular and clinical characterization of patients with overlapping 10p deletions. *Am. J. Med. Genet. A* **152A,** 1233–1243 (2010).
33 Elbracht, M., Roos, A., Schönherr, N., Busse, S., Damen, R., Zerres, K. *et al.* Pure distal trisomy 2q: a rare chromosomal abnormality with recognizable phenotype. *Am. J. Med. Genet. A* **149A,** 2547–2550 (2009).
34 Lukusa, T. & Fryns, J. P. Pure *de novo* 17q25.3 micro duplication characterized by micro array CGH in a dysmorphic infant with growth retardation, developmental delay and distal arthrogryposis. *Genet. Couns.* **21,** 25–34 (2010).
35 Fukami, M., Kirsch, S., Schiller, S., Richter, A., Benes, V., Franco, B. *et al.* A member of a gene family on Xp22.3, VCX-A, is deleted in patients with X-linked nonspecific mental retardation. *Am. J. Hum. Genet.* **67,** 563–573 (2000).
36 Shaffer, L. G. & Tommerup, N. *An International System for Human Cytogenetic Nomenclature (2005)* (Karger, Basel, 2005).
37 Koolen, D. A., Pfundt, R., de Leeuw, N., Hehir-Kwa, J. Y., Nillesen, W. M., Neefs, I. *et al.* Genomic microarrays in mental retardation: a practical workflow for diagnostic applications. *Hum. Mutat.* **30,** 283–292 (2009).
38 Miller, D. T., Adam, M. P., Aradhya, S., Biesecker, L. G., Brothman, A. R., Carter, N. P. *et al.* Consensus statement: chromosomal microarray is a first-tier clinical diagnostic test for individuals with developmental disabilities or congenital anomalies. *Am. J. Hum. Genet.* **86,** 749–764 (2010).
39 Shaffer, L. G., Theisen, A., Bejjani, B. A., Ballif, B. C., Aylsworth, A. S., Lim, C. *et al.* The discovery of microdeletion syndromes in the post-genomic era: review of the methodology and characterization of a new 1q41q42 microdeletion syndrome. *Genet. Med.* **9,** 607–616 (2007).
40 van Bon, B. W., Koolen, D. A., Borgatti, R., Magee, A., Garcia-Minaur, S., Rooms, L. *et al.* Clinical and molecular characteristics of 1qter microdeletion syndrome: delineating a critical region for corpus callosum agenesis/hypogenesis. *J. Med. Genet.* **45,** 346–354 (2008).
41 van Bon, B. W., Koolen, D. A., Brueton, L., McMullan, D., Lichtenbelt, K. D., Adès, L. C. *et al.* The 2q23.1 microdeletion syndrome: clinical and behavioural phenotype. *Eur. J. Hum. Genet.* **18,** 163–170 (2010).
42 Mencarelli, M. A., Kleefstra, T., Katzaki, E., Papa, F. T., Cohen, M., Pfundt, R. *et al.* 14q12 microdeletion syndrome and congenital variant of Rett syndrome. *Eur. J. Med. Genet.* **52,** 148–152 (2009).
43 Rump, P., Dijkhuizen, T., Sikkema-Raddatz, B., Lemmink, H. H., Vos, Y. J., Verheij, J. B. *et al.* Drayer's syndrome of mental retardation, microcephaly, short stature and absent phalanges is caused by a recurrent deletion of chromosome 15(q26.2→qter). *Clin. Genet.* **74,** 455–462 (2008).
44 Ballif, B. C., Hornor, S. A., Jenkins, E., Madan-Khetarpal, S., Surti, U., Jackson, K. E. *et al.* Discovery of a previously unrecognized microdeletion syndrome of 16p11.2-p12.2. *Nat. Genet.* **39,** 1071–1073 (2007).
45 Shinawi, M., Liu, P., Kang, S. H., Shen, J., Belmont, J. W., Scott, D. A. *et al.* Recurrent reciprocal 16p11.2 rearrangements associated with global developmental delay, behavioral problems, dysmorphism, epilepsy, and abnormal head size. *J. Med. Genet.* **47,** 332–341 (2010).
46 Kang, S. H., Scheffer, A., Ou, Z., Li, J., Scaglia, F., Belmont, J. *et al.* Identification of proximal 1p36 deletions using array-CGH: a possible new syndrome. *Clin. Genet.* **72,** 329–338 (2007).
47 Johnston, J. J., Olivos-Glander, I., Killoran, C., Elson, E., Turner, J. T., Peters, K. F. *et al.* Molecular and clinical analyses of Greig cephalopolysyndactyly and Pallister–Hall syndromes: robust phenotype prediction from the type and position of GLI3 mutations. *Am. J. Hum. Genet.* **76,** 609–622 (2005).
48 Johnston, J. J., Olivos-Glander, I., Turner, J., Aleck, K., Bird, L. M., Mehta, L. *et al.* Clinical and molecular delineation of the Greig cephalopolysyndactyly contiguous gene deletion syndrome and its distinction from acrocallosal syndrome. *Am. J. Med. Genet. A* **123A,** 236–242 (2003).
49 Hayashi, S., Okamoto, N., Makita, Y., Hata, A., Imoto, I. & Inazawa, J. Heterozygous deletion at 14q22.1-q22.3 including the BMP4 gene in a patient with psychomotor retardation, congenital corneal opacity and feet polysyndactyly. *Am. J. Med. Genet. A* **146A,** 2905–2910 (2008).
50 Hayashi, S., Mizuno, S., Migita, O., Okuyama, T., Makita, Y., Hata, A. *et al.* The CASK gene harbored in a deletion detected by array-CGH as a potential candidate for a gene causative of X-linked dominant mental retardation. *Am. J. Med. Genet. A* **146A,** 2145–2151 (2008).
51 Toyo-oka, K., Shionoya, A., Gambello, M. J., Cardoso, C., Leventer, R., Ward, H. L. *et al.* 14-3-3epsilon is important for neuronal migration by binding to NUDEL: a molecular explanation for Miller–Dieker syndrome. *Nat. Genet.* **34,** 274–285 (2003).
52 Mignon-Ravix, C., Cacciagli, P., El-Waly, B., Moncla, A., Milh, M., Girard, N. *et al.* Deletion of YWHAE in a patient with periventricular heterotopias and marked corpus callosum hypoplasia. *J. Med. Genet.* **47,** 132–136 (2010).
53 Haldeman-Englert, C. R., Gai, X., Perin, J. C., Ciano, M., Halbach, S. S., Geiger, E. A. *et al.* A 3.1-Mb microdeletion of 3p21.31 associated with cortical blindness, cleft lip, CNS abnormalities, and developmental delay. *Eur. J. Med. Genet.* **52,** 265–268 (2009).
54 Buysse, K., Delle Chiaie, B., Van Coster, R., Loeys, B., De Paepe, A., Mortier, G. *et al.* Challenges for CNV interpretation in clinical molecular karyotyping: lessons learned from a 1001 sample experience. *Eur. J. Med. Genet.* **52,** 398–403 (2009).
55 Fan, Y. S., Jayakar, P., Zhu, H., Barbouth, D., Sacharow, S., Morales, A. *et al.* Detection of pathogenic gene copy number variations in patients with mental retardation by genomewide oligonucleotide array comparative genomic hybridization. *Hum. Mutat.* **28,** 1124–1132 (2007).
56 Hevner, R. F., Shi, L., Justice, N., Hsueh, Y., Sheng, M., Smiga, S. *et al.* Tbr1 regulates differentiation of the preplate and layer 6. *Neuron* **29,** 353–366 (2001).
57 Cosma, M. P., Pepe, S., Annunziata, I., Newbold, R. F., Grompe, M., Parenti, G. *et al.* The multiple sulfatase deficiency gene encodes an essential and limiting factor for the activity of sulfatases. *Cell* **113,** 445–456 (2003).
58 Dierks, T., Schmidt, B., Borissenko, L. V., Peng, J., Preusser, A., Mariappan, M. *et al.* Multiple sulfatase deficiency is caused by mutations in the gene encoding the human C(alpha)-formylglycine generating enzyme. *Cell* **113,** 435–444 (2003).
59 Behar, O., Golden, J. A., Mashimo, H., Schoen, F. J. & Fishman, M. C. Semaphorin III is needed for normal patterning and growth of nerves, bones and heart. *Nature* **383,** 525–528 (1996).
60 Eudy, J. D., Ma-Edmonds, M., Yao, S. F., Talmadge, C. B., Kelley, P. M., Weston, M. D. *et al.* Isolation of a novel human homologue of the gene coding for echinoderm microtubule-associated protein (EMAP) from the Usher syndrome type 1a locus at 14q32. *Genomics* **43,** 104–106 (1997).
61 He, Y. & Casaccia-Bonnefil, P. The Yin and Yang of YY1 in the nervous system. *J. Neurochem.* **106,** 1493–1502 (2008).
62 Martin, C. L., Duvall, J. A., Ilkin, Y., Simon, J. S., Arreaza, M. G., Wilkes, K. *et al.* Cytogenetic and molecular characterization of A2BP1/FOX1 as a candidate gene for autism. *Am. J. Med. Genet.* **144B,** 869–876 (2007).
63 Tabolacci, E., Pomponi, M. G., Pietrobono, R., Terracciano, A., Chiurazzi, P. & Neri, G. A truncating mutation in the IL1RAPL1 gene is responsible for X-linked mental retardation in the MRX21 family. *Am. J. Med. Genet.* **140,** 482–487 (2006).
64 Nelson, J., Flaherty, M. & Grattan-Smith, P. Gillespie syndrome: a report of two further cases. *Am. J. Med. Genet.* **71,** 134–138 (1997).
65 Shaffer, L. G. & Bejjani, B. A. Medical applications of array CGH and the transformation of clinical cytogenetics. *Cytogenet. Genome Res.* **115,** 303–309 (2006).
66 Shaffer, L. G., Bejjani, B. A., Torchia, B., Kirkpatrick, S., Coppinger, J. & Ballif, B. C. The identification of microdeletion syndromes and other chromosome abnormalities: cytogenetic methods of the past, new technologies for the future. *Am. J. Med. Genet. C Semin. Med. Genet.* **145C,** 335–345 (2007).
67 Bejjani, B. A. & Shaffer, L. G. Clinical utility of contemporary molecular cytogenetics. *Annu. Rev. Genomics Hum. Genet.* **9,** 71–86 (2008).
68 Edelmann, L. & Hirschhorn, K. Clinical utility of array CGH for the detection of chromosomal imbalances associated with mental retardation and multiple congenital anomalies. *Ann. NY Acad. Sci.* **1151,** 157–166 (2009).
69 de Ståhl, T. D., Sandgren, J., Piotrowski, A., Nord, H., Andersson, R., Menzel, U. *et al.* Profiling of copy number variations (CNVs) in healthy individuals from three ethnic groups using a human genome 32K BAC-clone-based array. *Hum. Mutat.* **29,** 398–408 (2008).
70 Shao, L., Shaw, C. A., Lu, X. Y., Sahoo, T., Bacino, C. A., Lalani, S. R. *et al.* Identification of chromosome abnormalities in subtelomeric regions by microarray analysis: a study of 5,380 cases. *Am. J. Med. Genet. A* **146A,** 2242–2251 (2008).
71 Lu, X., Phung, M. T., Shaw, C. A., Pham, K., Neil, S. E., Patel, A. *et al.* Genomic imbalances in neonates with birth defects: high detection rates by using chromosomal microarray analysis. *Pediatrics* **122,** 1310–1318 (2008).
72 Xu, J. & Chen, Z. Advances in molecular cytogenetics for the evaluation of mental retardation. *Am. J. Med. Genet C Semin. Med. Genet.* **117C,** 15–24 (2003).
73 Ravnan, J. B., Tepperberg, J. H., Papenhausen, P., Lamb, A. N., Hedrick, J., Eash, D. *et al.* Subtelomere FISH analysis of 11 688 cases: an evaluation of the frequency and pattern of subtelomere rearrangements in individuals with developmental disabilities. *J. Med. Genet.* **43,** 478–489 (2006).
74 Ahn, J. W., Ogilvie, C. M., Welch, A., Thomas, H., Madula, R., Hills, A. *et al.* Detection of subtelomere imbalance using MLPA: validation, development of an analysis protocol, and application in a diagnostic centre. *BMC Med. Genet.* **8,** 9 (2007).
75 Schoumans, J., Ruivenkamp, C., Holmberg, E., Kyllerman, M., Anderlid, B. M. & Nordenskjold, M. Detection of chromosomal imbalances in children with idiopathic mental retardation by array based comparative genomic hybridisation (array-CGH). *J. Med. Genet.* **42,** 699–705 (2005).
76 de Vries, B. B., Pfundt, R., Leisink, M., Koolen, D. A., Vissers, L. E., Janssen, I. M. *et al.* Diagnostic genome profiling in mental retardation. *Am. J. Hum. Genet.* **77,** 606–616 (2005).
77 Rosenberg, C., Knijnenburg, J., Bakker, E., Vianna-Morgante, A. M., Sioos, W., Otto, P. A. *et al.* Array-CGH detection of micro rearrangements in mentally retarded individuals: clinical significance of imbalances present both in affected children and normal parents. *J. Med. Genet.* **43,** 180–186 (2006).
78 Krepischi-Santos, A. C., Vianna-Morgante, A. M., Jehee, F. S., Passos-Bueno, M. R., Knijnenburg, J., Szuhai, K. *et al.* Whole-genome array-CGH screening in undiagnosed syndromic patients: old syndromes revisited and new alterations. *Cytogenet. Genome Res.* **115,** 254–261 (2006).
79 Thuresson, A. C., Bondeson, M. L., Edeby, C., Ellis, P., Langford, C., Dumanski, J. P. *et al.* Whole-genome array-CGH for detection of submicroscopic chromosomal imbalances in children with mental retardation. *Cytogenet. Genome Res.* **118,** 1–7 (2007).
80 Wagenstaller, J., Spranger, S., Lorenz-Depiereux, B., Kazmierczak, B., Nathrath, M., Wahl, D. *et al.* Copy-number variations measured by single-nucleotide-polymorphism oligonucleotide arrays in patients with mental retardation. *Am. J. Hum. Genet.* **81,** 768–779 (2007).

81 Bruno, D. L., Ganesamoorthy, D., Schoumans, J., Bankier, A., Coman, D., Delatycki, M. *et al.* Detection of cryptic pathogenic copy number variations and constitutional loss of heterozygosity using high resolution SNP microarray analysis in 117 patients referred for cytogenetic analysis and impact on clinical practice. *J. Med. Genet.* **46,** 123–131 (2009).

82 Sagoo, G. S., Butterworth, A. S., Sanderson, S., Shaw-Smith, C., Higgins, J. P. & Burton, H. Array CGH in patients with learning disability (mental retardation) and congenital anomalies: updated systematic review and meta-analysis of 19 studies and 13,926 subjects. *Genet. Med.* **11,** 139–146 (2009).

83 Wincent, J., Anderlid, B. M., Lagerberg, M., Nordenskjöld, M. & Schoumans, J. High-resolution molecular karyotyping in patients with developmental delay and/or multiple congenital anomalies in a clinical setting. *Clin. Genet.* (e-pub ahead of print 8 May 2010).

84 Girirajan, S., Rosenfeld, J. A., Cooper, G. M., Antonacci, F., Siswara, P., Itsara, A. *et al.* A recurrent 16p12.1 microdeletion supports model for severe developmental delay. *Nat. Genet.* **42,** 203–209 (2010).

85 Veltman, J. A. & Brunner, H. G. Understanding variable expressivity in microdeletion syndromes. *Nat. Genet.* **42,** 192–193 (2010).

Reduced expression by *SETBP1* haploinsufficiency causes developmental and expressive language delay indicating a phenotype distinct from Schinzel–Giedion syndrome

Isabel Filges,[1] Keiko Shimojima,[2] Nobuhiko Okamoto,[3] Benno Röthlisberger,[4] Peter Weber,[5] Andreas R Huber,[4] Tsutomu Nishizawa,[6] Alexandre N Datta,[5] Peter Miny,[1] Toshiyuki Yamamoto[2]

► Additional figure and table are published online only. To view these files please visit the journal online (http://jmg.bmj.com).

[1]Division of Medical Genetics, University Children's Hospital and Department of Biomedicine, Basel, Switzerland
[2]Tokyo Women's Medical University Institute for Integrated Medical Sciences, Tokyo, Japan
[3]Osaka Medical Center and Research Institute for Maternal and Child health, Osaka, Japan
[4]Center of Laboratory Medicine, Cantonal Hospital, Aarau, Switzerland
[5]Division of Neuropediatrics and Developmental Medicine, University Children's Hospital, Basel, Switzerland
[6]Division of Virology, Department of Infectious and Immunity, Jichi Medical University School of Medicine, Shimotsuke, Japan

Correspondence to
Dr T Yamamoto, Tokyo Women's Medical University Institute for Integrated Medical Sciences, 8-1 Kawada-cho, Shinjuku-ward, Tokyo 162-8666, Japan; toshiyuki.yamamoto@twmu.ac.jp

Received 28 August 2010
Accepted 13 September 2010
Published Online First 30 October 2010

ABSTRACT

Background Mutations of the SET binding protein 1 gene (*SETBP1*) on 18q12.3 have recently been reported to cause Schinzel–Giedion syndrome (SGS). As rare 18q interstitial deletions affecting multiple genes including *SETBP1* correlate with a milder phenotype, including minor physical anomalies and developmental and expressive speech delay, mutations in *SETBP1* are thought to result in a gain-of-function or a dominant-negative effect. However, the consequence of the *SETBP1* loss-of-function has not yet been well described.

Methods Microarray-based comparative genomic hybridisation (aCGH) analyses were performed to identify genetic causes for developmental and expressive speech delay in two patients. SETBP1 expression in fibroblasts obtained from one of the patients was analysed by real-time RT-PCR and western blotting. A cohort study to identify nucleotide changes in *SETBP1* was performed in 142 Japanese patients with developmental delay.

Results aCGH analyses identified submicroscopic deletions of less than 1 Mb exclusively containing *SETBP1*. Both patients show global developmental, expressive language delay and minor facial anomalies. Decreased expression of SETBP1 was identified in the patient's skin fibroblasts. No pathogenic mutation of *SETBP1* was identified in the cohort study.

Conclusion SETBP1 expression was reduced in a patient with *SETBP1* haploinsufficiency, indicating that the *SETBP1* deletion phenotype is allele dose sensitive. In correlation with the exclusive deletion of *SETBP1*, this study delimits a milder phenotype distinct from SGS overlapping with the previously described phenotype of del(18)(q12.2q21.1) syndrome including global developmental, expressive language delay and distinctive facial features. These findings support the hypothesis that mutations in *SETBP1* causing SGS may have a gain-of-function or a dominant-negative effect, whereas haploinsufficiency or loss-of-function mutations in *SETBP1* cause a milder phenotype.

Mutations in the SET binding protein 1 gene (*SETBP1*) have recently been shown to cause Schinzel–Giedion syndrome (SGS, MIM #269150).[1] Whole-exome sequencing for four patients with SGS identified nucleotide alterations in the conserved region of *SETBP1*. Further analyses by standard Sanger sequencing for nine patients with SGS were performed, and eight of the nine patients showed *SETBP1* mutations. All five identified mutations were missense mutations, rather than nonsense mutations or truncations. As previously reported, rare chromosomal deletions in 18q including *SETBP1* correlate with a milder phenotype, and the severe SGS phenotype was proposed to be the consequence of a gain-of-function or dominant-negative effect of the mutations. However, the exact function of the gene is not known, and the consequences of an exclusive *SETBP1* loss-of-function or haploinsufficiency are not well described.

We identified de novo heterozygous microdeletions containing exclusively *SETBP1* in two patients with developmental, expressive language delay and distinctive facial features. The phenotypes are milder and differ significantly from the severe clinical appearance of SGS. Genotype–phenotype correlations of *SETBP1* haploinsufficiency are demonstrated in this study and discussed.

PATIENTS AND METHODS

Patients

After informed consent based on permission from the ethics committee of the institutions or individual written consent had been obtained, peripheral blood samples were taken from patients with developmental delay of unidentified aetiology to investigate potential genomic copy number aberrations.

Patients' reports

Patient 1 (DECIPHER #TWM253969) is a 7-year old boy, the second child of non-consanguineous parents (https://decipher.sanger.ac.uk/). His 10-year-old sister is healthy and normally developed. He was born with a birth weight of 2504 g (3–10th centile), length of 47 cm (10–25th centile), and occipitofrontal circumference (OFC) of 33.5 cm (=50th centile). At the time of his birth, his father and mother were 34 and 40 years old, respectively. His development was moderately delayed with crawling at 1 year, free walking at 2 years, and the first word at 5 years. He suffered febrile seizures several times, but EEG and brain MRI showed no abnormal findings. At 7 years, his height was 115 cm (25–50th centile), weight was 15.0 kg (<3rd centile), and OFC was 49.3 cm (3–10th centile). He showed distinctive facial features with an inverted triangle face, prominent forehead, ptosis with periorbital fullness, epicanthus and

pointed chin (figure 1A). He can walk by himself and can speak only a few words. The Kyoto developmental scale measured his developmental quotient as 40, which indicated moderate developmental delay. Visual acuity examination showed a refractive error of +8D in both eyes, indicating hyperopia. Previously performed conventional chromosomal analysis showed a normal male karyotype of 46,XY.

Patient 2, the 3rd child of non-consanguineous healthy parents, was born at 38 weeks by caesarean section for breech presentation after an uneventful pregnancy. In the neonatal period, the boy was hypotonic, sleepy and passive and rarely cried. He showed significantly delayed motor development, with sitting at 14 months and walking at 2 years, as well as delayed pincer grip. Initially, a discrete hemiparesis of the left part of his body manifested only while running with a slight spastic posture of his left hand and gait asymmetry suggested a perinatal or prenatal stroke. Cerebral MRI at the age of 4 years was normal except an unspecific T2 hyperintense infratentorial lesion in the right cranial paramedian cerebellum. The patient still exhibits coordination deficits in fine motoricity. His growth parameters are in the normal range (75th–90th centile), and OFC is within the 10th–25th centile. Hearing was found to be normal. Interestingly, the boy has not developed any expressive speech at all to date, whereas receptive language abilities are intact. He actively communicates using gestures illustrating his demands and ideas, but well understands his interlocutor, permitting a bidirectional exchange. He exhibits kind and social behaviour but at the same time a restless search for interactive communication. He has difficulty concentrating and has no sense of danger or pain. Facial dysmorphisms include frontal upsweep, a lighter blond hair corona in the front, hypertelorism, ptosis of eyelids predominantly on the left, periorbital fullness, straight and sparse eyebrows, flat nasal bridge, short nose, thin upper lip, short fingers and broad distal phalanges (figure 1B–D). No major malformations have been found. Microcytic hypochrome anaemia remains unexplained; the search for HbH inclusion bodies which would indicate X-linked α-thalassaemia/mental retardation syndrome was negative.

Microarray-based comparative genomic hybridisation (aCGH)

aCGH analyses were performed using the Human Genome CGH Microarray 44K (Agilent Technologies, Santa Clara, California, USA) and the whole genome tiling NimbleGen CGH array (Human CGH 2.1M WG-T v2.0; NimbleGen; Roche NimbleGen Inc, Madison, Wisconsin, USA) for patient 1 and patient 2, respectively, according to the manufacturer's protocols.

Fluorescence in situ hybridisation

Identified aberrations were confirmed by fluorescence in situ hybridisation (FISH) using locus-specific BAC clones as probes. In patient 1, two clones, CTD-3236P11 on 18q12.3 (chr18:40 779 351–40 864 576) as a target and RP11-105C15 on 18p11.31 (chr18:5 910 725–60 63 460) as a marker, were selected from the UCSC genome browser (http://www.genome.ucsc.edu). In patient 2, the locus-specific probe RP11-24L5 (BlueGnome, Cambridge, UK) in the region 18q12.3 (chr18:40 588 784–40 776 858) was used on metaphase spreads. Physical positions refer to the March 2006 human reference sequence (NCBI Build 36.1).

Expression analysis of SETBP1

Total RNAs were extracted from cultured skin fibroblasts from patient 1 and the control individual using the ISOGEN RNA extraction kit (Wako, Osaka, Japan), reverse-transcribed to complementary DNA (cDNA) using the SuperScript VILO cDNA Synthesis Kit (Life Technologies, Carlsbad, California, USA) according to the manufacturer's instructions, then used as templates for real-time PCR using Power SYBR Green PCR master mix (Life Technologies). Primers for SETBP1 mRNA were designed in the coding region (SETBP1 nt374F; 5′-GTCCA CCTGAGATCAAGATC-3′ and SETBP1 nt663R; 5′-GTCCATGT GGTTCTGGCTGC-3′). Beta actin primers (5′-GGCACCCAGCA CAATGAAGATC-3′ and 5′-AAGTCATAGTCCGCCTAGAAGC-3′)

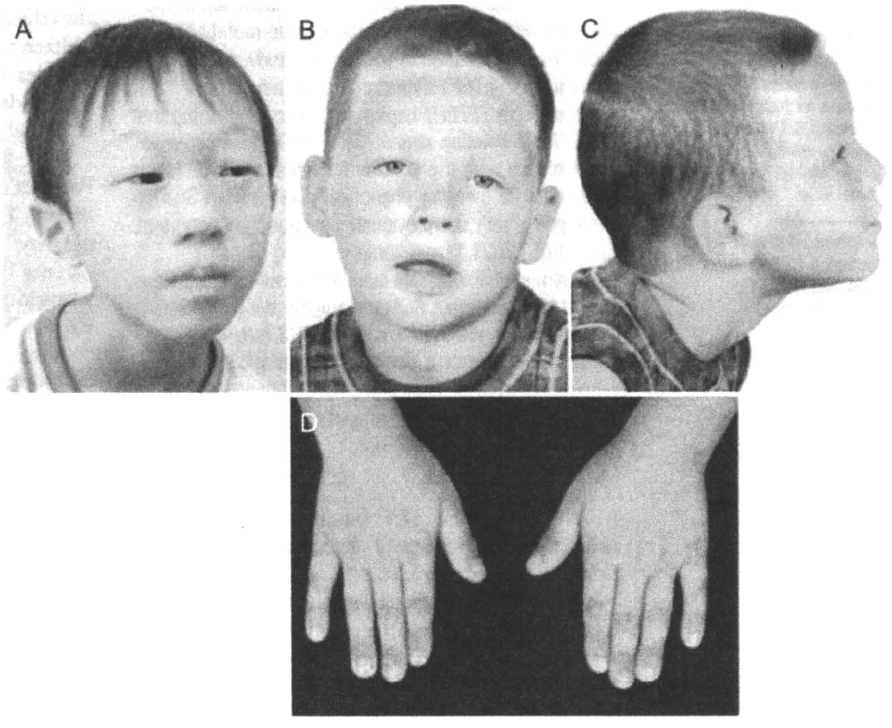

Figure 1 Phenotypes of the patients. (A) Patient 1; (B,C) frontal and lateral views of patient 2; (D) both hands of patient 2.

were used for the internal control. Real-time PCR amplifications were performed in three independent replicates on an ABI7500 (Life Technologies), and the data were evaluated by the Delta Delta Ct method.[2] The SETBP1 expression ratio (patient versus normal control) was calculated in each of the three examinations.

Concentrations of SETBP1 in the cell lysates of skin fibroblasts from patient 1 and the control were also analysed by western blotting using the SETBP1 MaxPab mouse polyclonal antibody (B01), catalogue number H00026040-B01 (Abnova, Taipei City, Taiwan) as described previously.[3]

Cohort study of *SETBP1*

A total of 142 Japanese patients with developmental delay, without genomic copy number aberrations as determined by aCGH, participated in the cohort study.[4] *SETBP1* sequences were analysed by the standard PCR-direct sequencing method. The primers used for PCR and the big-dye sequencing reaction (Life Technologies) were designed using Primer3 (http://primer3.sourceforge.net/) (supplemental online table 1). When we identified nucleotide changes in samples for which parental samples were available, trio analyses were performed to check whether the changes were de novo or familial. The nucleotide sequences of *SETBP1*, in which nucleotide alterations were found in the cohort study, were compared with homologues in species including *Callithrix jacchus*, *Gorilla gorilla*, *Macaca mulatta*, *Pan troglodytes*, *Pongo pygmaeus*, *Tarsius syrichta* and *Tupaia belangeri*, which were identified using Gene Tree (http://www.ensembl.org). DNA samples from 70 Japanese volunteers were used for the control cohort of normal Japanese.

RESULTS

Cytogenetic analyses

In patient 1, aCGH analysis revealed an aberration in the contiguous 11 probes at 18q12.3 with the mean $\log_2$ ratio of −1.02306 (figure 2A). This indicated a 986 kb loss of genomic copy number at 18q12.3; molecular karyotyping was determined as arr chr18q12.3q12.3 (40 282 934–41 269 199)x1. The deletion exclusively contained *SETBP1* and was confirmed by FISH analysis showing only one signal from the targeted probes (supplemental online figure S1). FISH analysis using the same probes showed no abnormality in either parent, indicating a de novo deletion (data not shown).

In patient 2, aCGH showed an 850 kb deletion within the chromosomal region 18q12.3 (chr18:40 233 803–41 088 224) (figure 2B). The deletion was confirmed by FISH, and both parents were found to be normal by conventional chromosome analysis and FISH analysis with the same locus-specific probe, indicating a de novo occurrence (data not shown). The only referenced gene within the deleted region was *SETBP1*. The two neighbouring genes, *BC051727* and *AK123972*, were non-coding. *TSLC14A2* (NM_007163) encodes a renal tubular urea transporter of the solute carrier family 14, not related to the phenotype of the patient.

Expression of SETBP1

In comparison with the normal control, SETBP1 RNA expression in the skin fibroblasts derived from patient 1 was reduced to 0.53, 0.60 and 0.41 (mean 0.51), and the lower SETBP1

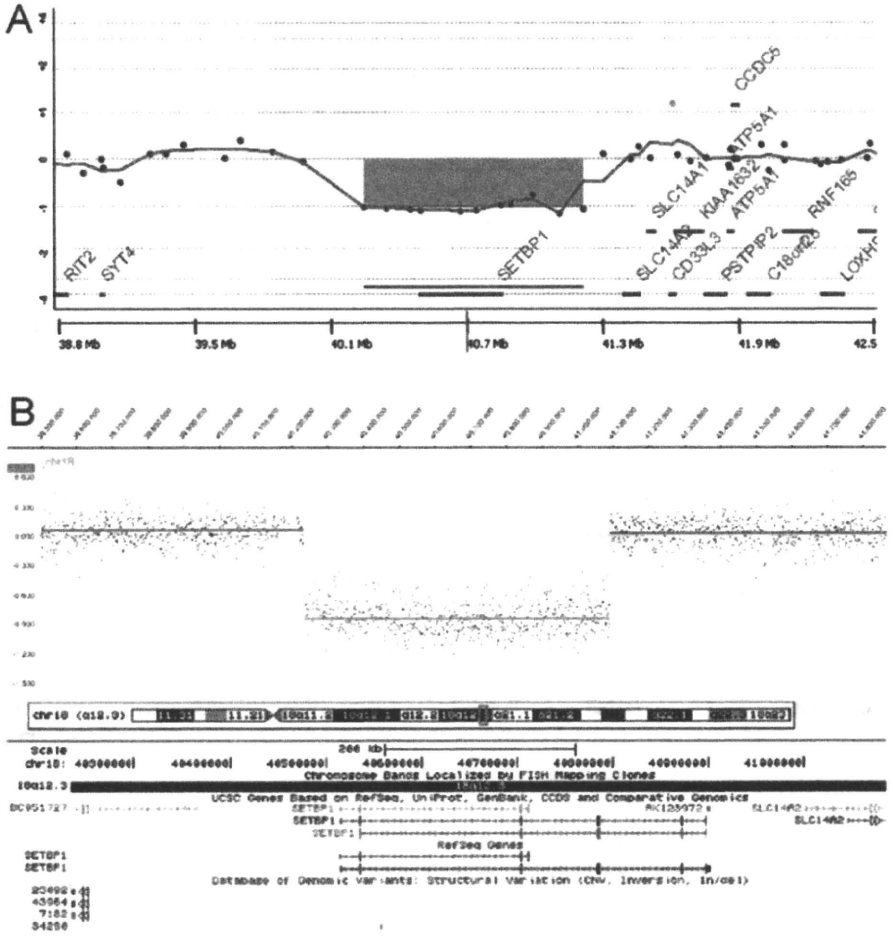

Figure 2 Microarray-based comparative genomic hybridisation identifies small deletions including *SETBP1* in patient 1 (A) and patient 2 (B). DNA copy number changes are represented by the negative $\log_2$ ratio below the baseline showing the deletions. (B) The square in the chromosome ideogram indicates the chromosomal position of the deletion; genes contained within the deletion are depicted below (http://genome.ucsc.edu).

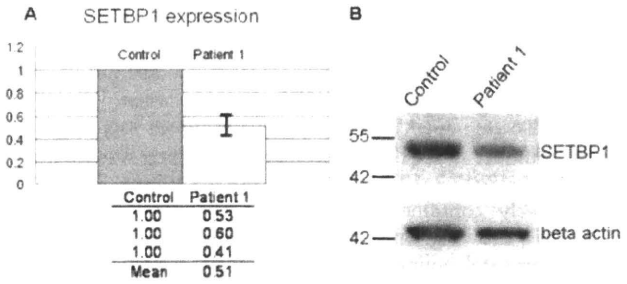

Figure 3 Expression studies. (A) SETBP1 RNA expression ratio analysed by real-time PCR. Raw data are given beneath the histogram. SETBP1 expression in the patient was about half that found in the control. (B) Western blotting of SETBP1. A total of 10 μg protein was separated in the gels. SETBP1 protein can be seen to be decreased in the patient. Beta actin was used as the internal control. Molecular mass (kDa) is indicated on the left of the gel.

protein concentration was also confirmed by western blotting (figure 3A,B).

Cohort study for *SETBP1* mutations

We identified 18 nucleotide changes including 11 non-synonymous and seven synonymous mutations, but no nonsense and no truncation mutations (table 1). The seven synonymous and four non-synonymous mutations, V231L, A390V, V1101I and P1130T, which were already listed in the single-nucleotide polymorphism database, were benign single-nucleotide polymorphisms. Four missense mutations (R627C, E958G, G1067S and W1242C; data not shown) located on the conserved sequence regions compared with the homologous genes from other species were not identified in normal control samples. However, W1242C was found in a healthy parent. Q1558L was also inherited from a healthy parent. The codon positions of E1466D and P1526Q were conserved among species and included in the important regions, SET-binging region and PPLPPPPP repeat, respectively. However, the patients' phenotypes were not similar to the presenting patient or SGS. Thus there was no definite pathogenic mutation. The sequence of the remaining *SETBP1* allele in patient 1 contained no nucleotide alterations.

DISCUSSION

In this study, we identified two patients with de novo chromosomal microdeletions in 18q12.3 that included *SETBP1* exclusively. *SETBP1* haploinsufficiency was suggested to be pathogenic. The patients exhibit moderate developmental delay and distinctive facial features, including prominent forehead, sparse eyebrows, mild ptosis with periorbital fullness. Patient 2 in particular showed a striking discrepancy between expressive speech impairment and conserved receptive speech, which has also been previously observed in patients with larger deletions in del(18)(q12.3q12.3). The complete and exclusive loss of one copy of *SETBP1* in our patient in correlation thus suggests an essential role for *SETBP1* in expressive speech development.

Schinzel *et al* reported on three patients with del(18)(q12.2q21.1) showing muscular hypotonia, seizures, behavioural disorders, and a pattern of minor dysmorphic features including prominent forehead, ptosis of the upper eyelids, full periorbital tissue, epicanthic folds and strabismus.[5] These phenotypic characteristics are similar to those in the cases presented here. Tinkle *et al* reported on a patient with del(18)(q12.2q21.1) with

Table 1 Identified nucleotide alteration in the cohort study

Nucleotide position*	Change	Amino acid change*	Location	Number of alleles that showed nucleotide changes	Conserved/ not conserved†	Function‡	Trio analyses	Results of population study	In silico database
c. 691	G>C	V231L	Exon 4	4	Not conserved				rs11082414
c. 1169	C>T	A390V	Exon 4	1	Not conserved				rs8091231
c. 1879	C>T	R627C	Exon 4	3	Conserved			None	None
c. 1911	G>A	P637P (synonymous)	Exon 4	1	-				None
c. 1932	C>T	S644S (synonymous)	Exon 4	2	-				rs3744824
c. 2607	C>T	S869S (synonymous)	Exon 4	12	-	The Ski homology region			None
c. 2873	A>G	E958G	Exon 4	1	Conserved			None	None
c. 3199	G>A	G1067S	Exon 4	1	Conserved			None	None
c. 3301	G>A	V1101I	Exon 4	90	Conserved				rs3744825
c. 3372	C>T	G1124G (synonymous)	Exon 4	1	-				None
c. 3388	C>A	P1130T	Exon 4	66	Conserved				rs1064204
c. 3726	G>C	W1242C	Exon 4	1	Conserved		Familial	None	None
c. 3825	A>G	S1275S (synonymous)	Exon 4	2	-				rs8096662
c. 4010	G>C	S1337S (synonymous)	Exon 5	1	-	SET-binding region			None
c. 4398	G>T	E1466D	Exon 6	3	Conserved	SET-binding region			None
c. 4563	C>G	P1521P (synonymous)	Exon 6	1	-	PPLPPPPP repeat			None
c. 4577	C>A	P1526Q	Exon 6	1	Conserved	PPLPPPPP repeat			None
c. 4673	A>T	Q1558L	Exon 6	1	Conserved		Familial		None

*Nucleotide and amino acid positions indicate NM_015559 sequence with the first initiation codon ATG at position 1.
†Conserved or not conserved was determined by comparison with the other species.
‡Functional domains were obtained from Minakuchi *et al* (2001).[12]

long-term survival, and concluded that life expectancy is minimally reduced.[6]

Although the previously reported chromosomal anomalies were identified at chromosomal G-banded levels, in more recent reports deletions in 18q12.2q21.1 were characterised by molecular techniques, and common features in the patients' phenotypes were reported.[7 8] The critical region for the phenotype of patients was narrowed to the 18q12.3-q21.1 region by Cody *et al*[9] and Buysse *et al*[10] (figure 4), who proposed a new syndrome involving expressive speech delay. They hypothesised that genes within the region may be specific to the neural and motor planning domains necessary for speech. However, deletions described so far contain numerous genes, including *SETBP1*, not allowing a phenotype–genotype correlation for haploinsufficiency of *SETBP1* exclusively.

Our findings correlate the phenotypes of the two patients with the exclusive complete loss of one copy of *SETBP1*. There is significant phenotypic overlap with the previously reported del (18)(q12.2q21.1) syndrome, suggesting a major contribution of the deletion of *SETBP1* to these phenotypes, as it has been described in contiguous deletion syndromes. The discrepancy between expressive and receptive language abilities in our patients appears to be a unique characteristic in the *SETBP1* deletion phenotype. The complete and exclusive loss of one copy of *SETBP1* in our patients in correlation with their phenotypes suggests an essential role for *SETBP1* in expressive speech development, although the exact function of the gene remains unknown.

SETBP1 encodes SET binding protein 1 expressed in numerous tissues including fetal brain. Its fusion with nucleoporin 98 kDa (*NUP98*) by chromosomal translocation has been shown in acute T-cell lymphoblastic leukaemia,[11] and the SET binding protein has been proposed to play a key role in the mechanism of SET-related leukaemogenesis and tumorigenesis by regulatory function in the nucleus.[12] Hoischen *et al* recently identified mutations in *SETBP1* to be causative of SGS, which is

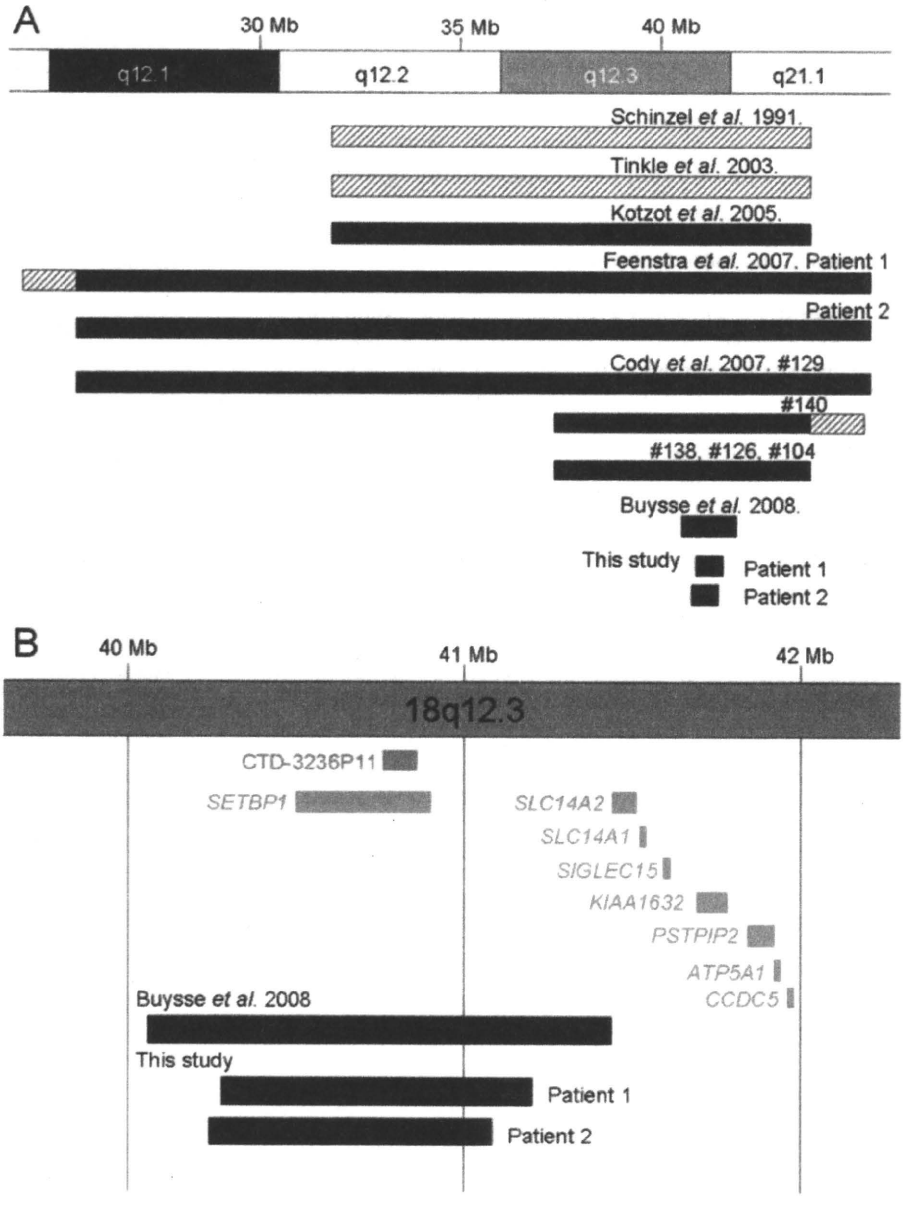

Figure 4 Comparison of the deletion regions. (A) Schematic representation of the previously reported deletions on a physical map of chromosome 18. (B) The deletion region of the patient is expanded. Bars filled with black and diagonal lines indicate definite and ambiguous deletion regions, respectively. Green and red bars indicate the position of the BAC clone used for fluorescence in situ hybridisation and the known genes, respectively.

characterised by severe mental retardation, distinctive facial features, and multiple congenital malformations.[1] Prognosis is poor, and most affected individuals die in the first decade of life. All reported mutations of *SETBP1* in patients with SGS were missense mutations in the important SET-binding region, and a gain-of-function or dominant-negative effect was suspected.[12]

As the phenotype of our two patients and the previously reported patients with del(18)(q12.2q21.1) including *SETBP1* does not resemble SGS and clinical features are generally milder, we conclude that haploinsufficiency of *SETBP1* does not cause SGS. We analysed the expression of SETBP1 by real-time PCR and western blotting, and found that SETBP1 was reduced in patient-derived skin fibroblasts, confirming that the effects of SETBP1 are allele dose-dependent. The deletion mainly affects speech, but the syndromic phenotype includes global development delay and recognisable facial dysmorphism underlying ubiquitous expression of SETBP1. As the phenotypic appearance of *SETBP1* haploinsufficiency is completely different from that of SGS, our findings support the proposed gain-of-function or dominant negative effect of the identified mutations in this gene.

There are various examples of phenotypic variability due to the different nature of mutations in the same gene. Mutations in fibroblast growth factor 3 (*FGFR3*) cause disproportionate growth in achondroplasia by gain-of-function, whereas terminal deletions of 4p including *FGFR3* cause Wolff–Hirschhorn syndrome, which does not show disproportionate growth at all, but small stature.[13 14] On the other hand, gain-of-function mutations of T-box 1 (*TBX1*) can result in the same phenotypic spectrum as haploinsufficiency caused by loss-of-function mutations or deletions in 22q11 including *TBX1*.[15]

In our study, we delimit a phenotype for haploinsufficiency of *SETBP1* distinct from the phenotype of SGS described in patients with mutations in the same gene suggesting a gain-of-function or a dominant negative effect of the mutations described. The *SETBP1* deletion phenotype seems to overlap extensively with the previously described del(18)(q12.2q21.1) syndrome, which has been characterised by moderate developmental delay, distinctive facial appearance, expressive language delay, and behavioural problems. Haploinsufficiency of *SETBP1* may thus primarily contribute to the phenotype of this contiguous gene syndrome. We did not identify pathogenic mutations on sequencing *SETBP1* in a cohort of 142 patients with developmental delay. Additional studies of the exact cellular function of *SETBP1* are needed to understand the pathogenic origin of the variable and distinct phenotypes.

Acknowledgements We thank the patients' parents for their gracious participation and support. We are grateful to the technicians from our laboratories, including Ms Etsuko Tanji, for their skilful help. We also acknowledge the DECIPHER database for comparing our data with those of others.

Funding This work was partially supported by a research grant from the University of Basel (DMS2058) and the Japan Ministry of Education, Science, Sports and Culture, Grant-in-Aid for Scientific Research (C), 21591334, 2010.

Competing interests None.

Patient consent Obtained.

Ethics approval This study was conducted with the approval of the Tokyo Women's Medical University and the University of Basel.

Provenance and peer review Not commissioned; externally peer reviewed.

REFERENCES

1. **Hoischen A,** van Bon BW, Gilissen C, Arts P, van Lier B, Steehouwer M, de Vries P, de Reuver R, Wieskamp N, Mortier G, Devriendt K, Amorim MZ, Revencu N, Kidd A, Barbosa M, Turner A, Smith J, Oley C, Henderson A, Hayes IM, Thompson EM, Brunner HG, de Vries BB, Veltman JA. De novo mutations of SETBP1 cause Schinzel-Giedion syndrome. *Nat Genet* 2010;**42**:483–5.
2. **Schefe JH,** Lehmann KE, Buschmann IR, Unger T, Funke-Kaiser H. Quantitative real-time RT-PCR data analysis: current concepts and the novel "gene expression's CT difference" formula. *J Mol Med* 2006;**84**:901–10.
3. **Shimojima K,** Komoike Y, Tohyama J, Takahashi S, Paez MT, Nakagawa E, Goto Y, Ohno K, Ohtsu M, Oguni H, Osawa M, Higashinakagawa T, Yamamoto T. TULIP1 (RALGAPA1) haploinsufficiency with brain development delay. *Genomics* 2009;**94**:414–22.
4. **Komoike Y,** Shimojima K, Liang JS, Fujii H, Maegaki Y, Osawa M, Fujii S, Higashinakagawa T, Yamamoto T. A functional analysis of GABARAP on 17p13.1 by knockdown zebrafish. *J Hum Genet* 2010;**55**:155–62.
5. **Schinzel A,** Binkert F, Lillington DM, Sands M, Stocks RJ, Lindenbaum RH, Matthews H, Sheridan H. Interstitial deletion of the long arm of chromosome 18, del (18)(q12.2q21.1): a report of three cases of an autosomal deletion with a mild phenotype. *J Med Genet* 1991;**28**:352–5.
6. **Tinkle BT,** Christianson CA, Schorry EK, Webb T, Hopkin RJ. Long-term survival in a patient with del(18)(q12.2q21.1). *Am J Med Genet A* 2003;**119A**:66–70.
7. **Kotzot D,** Haberlandt E, Fauth C, Baumgartner S, Scholl-Burgi S, Utermann G. Del (18)(q12.2q21.1) caused by a paternal sister chromatid rearrangement in a developmentally delayed girl. *Am J Med Genet A* 2005;**135**:304–7.
8. **Feenstra I,** Vissers LE, Orsel M, van Kessel AG, Brunner HG, Veltman JA, van Ravenswaaij-Arts CM. Genotype-phenotype mapping of chromosome 18q deletions by high-resolution array CGH: an update of the phenotypic map. *Am J Med Genet A* 2007;**143A**:1858–67.
9. **Cody JD,** Sebold C, Malik A, Heard P, Carter E, Crandall A, Soileau B, Semrud-Clikeman M, Cody CM, Hardies LJ, Li J, Lancaster J, Fox PT, Stratton RF, Perry B, Hale DE. Recurrent interstitial deletions of proximal 18q: a new syndrome involving expressive speech delay. *Am J Med Genet A* 2007;**143A**:1181–90.
10. **Buysse K,** Menten B, Oostra A, Tavernier S, Mortier GR, Speleman F. Delineation of a critical region on chromosome 18 for the del(18)(q12.2q21.1) syndrome. *Am J Med Genet A* 2008;**146A**:1330–4.
11. **Panagopoulos I,** Kerndrup G, Carlsen N, Strombeck B, Isaksson M, Johansson B. Fusion of NUP98 and the SET binding protein 1 (SETBP1) gene in a paediatric acute T cell lymphoblastic leukaemia with t(11;18)(p15;q12). *Br J Haematol* 2007;**136**:294–6.
12. **Minakuchi M,** Kakazu N, Gorrin-Rivas MJ, Abe T, Copeland TD, Ueda K, Adachi Y. Identification and characterization of SEB, a novel protein that binds to the acute undifferentiated leukemia-associated protein SET. *Eur J Biochem* 2001;**268**:1340–51.
13. **Richette P,** Bardin T, Stheneur C. Achondroplasia: from genotype to phenotype. *Joint Bone Spine* 2008;**75**:125–30.
14. **Altherr MR,** Wright TJ, Denison K, Perez-Castro AV, Johnson VP. Delimiting the Wolf-Hirschhorn syndrome critical region to 750 kilobase pairs. *Am J Med Genet* 1997;**71**:47–53.
15. **Zweier C,** Sticht H, Aydin-Yaylagul I, Campbell CE, Rauch A. Human TBX1 missense mutations cause gain of function resulting in the same phenotype as 22q11.2 deletions. *Am J Hum Genet* 2007;**80**:510–7.

RESEARCH ARTICLE

AMERICAN JOURNAL OF medical genetics PART A

Characterization of a De Novo Balanced t(4;20)(q33;q12) Translocation in a Patient With Mental Retardation

Kenichiro Yamada,[1] Daisuke Fukushi,[1] Takao Ono,[1] Yoko Kondo,[1,2] Reiko Kimura,[1] Noriko Nomura,[1] Ken-jiro Kosaki,[3] Yasukazu Yamada,[1] Seiji Mizuno,[4] and Nobuaki Wakamatsu[1]*

[1]Department of Genetics, Institute for Developmental Research, Aichi Human Service Center, Kasugai, Aichi, Japan

[2]Department of Pediatrics, Nagoya University Graduate School of Medicine, Nagoya, Japan

[3]Department of Pediatrics, Keio University, Tokyo, Japan

[4]Department of Pediatrics, Central Hospital, Aichi Human Service Center, Kasugai, Aichi, Japan

Received 8 May 2009; Accepted 28 August 2009

CHD6 is an ATP-dependent chromatin-remodeling enzyme, which has been implicated as a crucial component for maintaining and regulating chromatin structure. CHD6 belongs to the largest subfamily, subfamily III (CHD6–9), of the chromodomain helicase DNA (CHD-binding protein) family of enzymes (CHD1–9). Here we report on a female patient with a balanced translocation t(4;20)(q33;q12) presenting with severe mental retardation and brachydactyly of the toes. We identified the translocation breakpoint in intron 27 of *CHD6* at 20q12, while the 4q33 breakpoint was intergenic. Northern blot analysis demonstrated the *CHD6* mRNA in the patient's lymphoblastoid cells was decreased to ~50% of the control cells. To investigate the cellular mechanism of diseases resulting from decreased CHD subfamily III proteins, we knocked down CHD6 or CHD7 by RNA interference in HeLa cells and analyzed chromosome alignment. The both CHD6- and CHD7-knockdown cells showed increased frequency of misaligned chromosomes on metaphase plates. Moreover, an elevated frequency of aneuploidy, the major cause of miscarriages and mental retardation, was observed in patients with *CHD6* and *CHD7* haploinsufficiency. These results suggest that CHD6 and CHD7 play important roles in chromatin assembly during mitosis and that mitotic delay and/or impaired cell proliferation may be associated with pathogenesis of the diseases caused by *CHD6* or *CHD7* mutations.

Key words: CHD6; CHD7; mental retardation; brachydactyly; chromosome 20; translocation; chromatin assembly; chromosome alignment

How to Cite this Article:
Yamada K, Fukushi D, Ono T, Kondo Y, Kimura R, Nomura N, Kosaki K-j, Yamada Y, Mizuno S, Wakamatsu N. 2010. Characterization of a de novo balanced t(4;20)(q33;q12) translocation in a patient with mental retardation.
Am J Med Genet Part A 152A:3057–3067.

INTRODUCTION

Chromodomain helicase DNA (CHD) proteins are members of the SWI2/SNF2-related ATPase superfamily and feature a combination of functional chromatin organization modifier, SNF2-related helicase/ATPase, and/or DNA-binding domains [Woodage et al., 1997]. On the basis of sequence conservation and phylogenetic divergence of the SNF2-related helicase/ATPase domains, Schuster and Stoger [2002] divided the 9-member CHD family into three subfamilies. Only the subfamily I members, CHD1 and CHD2, appear to have DNA binding domains [Stokes and Perry, 1995]. CHD3, CHD4, and CHD5 are grouped into subfamily II, and the remainder (CHD6–9) constitute subfamily III.

CHDs of subfamily III are larger than the other CHDs and have been proposed to contain additional motifs or domains. *CHD7* (GenBank accession number NM_017780) was identified as a causal gene for the CHARGE syndrome, a genetic disorder characterized by coloboma of the eye (C), heart anomalies (H), choanal atresia (A), retardation of mental and somatic development

Additional supporting information may be found in the online version of this article.

Grant sponsor: Uehara Memorial Foundation; Grant sponsor: Ministry of Education, Culture, Sports, Science and Technology of Japan.

*Correspondence to:
Nobuaki Wakamatsu, Department of Genetics, Institute for Developmental Research, Aichi Human Service Center, 713-8 Kamiya-cho, Kasugai, Aichi 480-0392, Japan. E-mail: nwaka@inst-hsc.jp

Published online 5 November 2010 in Wiley Online Library (wileyonlinelibrary.com).
DOI 10.1002/ajmg.a.33174

(R), genital anomalies (G), and ear abnormalities and/or deafness (E) [Vissers et al., 2004]. CHD8 interacts with chromatin insulator binding protein CTCF; the CTCF–CHD8 complex contributes to the insulation and epigenetic regulation of chromatin [Ishihara et al., 2006]. CHD8 also associates with Staf transcription factor and contributes to efficient U6 RNA polymerase III transcription [Yuan et al., 2007]. CHD9 (CreMM) regulates transcription during the differentiation of osteogenic cells [Shur and Benayahu, 2005; Shur et al., 2006].

CHD6 (GenBank accession number NM_032221), formerly identified as CHD5, also belongs to subfamily III [Schuster and Stoger, 2002]. A recent study showed that it has DNA-dependent ATPase activity and co-localizes with hypo- and hyper-phosphorylated forms of RNA-polymerase II which implies that it may function as a chromatin-remodeling factor similarly to CHD1 [Lutz et al., 2006]. To date, no mutations in *CHD6* have been associated with any genetic disease.

Here we report on a female patient with severe mental retardation and brachydactyly of the toes accompanied by a balanced translocation t(4;20)(q33;q12). The translocation breakpoint of 20q12 was found to be localized within *CHD6* and a decrease in the steady-state level of *CHD6* mRNA was evident in the patient's lymphoblastoid cells. We also analyzed chromosome alignment following knockdown of CHD subfamily III (CHD6 or CHD7) in HeLa cells and determined chromosome numbers of lymphoblastoid cells of the patients in an effort to determine the cellular mechanism of disease caused by CHD6 or CHD7 haploinsufficiency.

MATERIALS AND METHODS

Bioethics Approval

With the approval of the ethics committee of Aichi Human Service Center, whole blood of patients and unaffected individuals was collected after written informed consent was obtained.

Patients and Cell Lines

Patient 1: The patient is a 16-year-old Japanese female, born to healthy non-consanguineous parents (30-year-old mother and 33-year-old father). The birth was at 37 weeks gestation without any complications with a body weight of 3,700 g (+1.5 SD), length of 48.0 cm (−0.2 SD), and an occipitofrontal circumference (OFC) of 36 cm (−0.8 SD). She is the second child. Her motor milestones were head control at 5 months, sitting at 8 months, speaking a few words at 18 months, and walking without support at 25 months. General muscle tone was mildly decreased during early infancy. She was admitted to Central Hospital of Aichi Human Service Center for further evaluation at 5 months because of delayed milestones and no social smiling. At this time, routine laboratory examinations did not lead to any abnormal findings. Brain MRI at 3 years of age revealed slightly dilated ventricles, but the results of electroencephalography (EEG) were normal. Her intelligence quotient (IQ) was 29 at age 5. At 8 years of age, gray hair was slightly remarkable. At age 11, karyotype analysis with standard G banding was performed and she was found to have a translocation of t(4;20)(q33;q12) (Fig. 1E). At present, her IQ is 17 and her height, weight, and OFC are

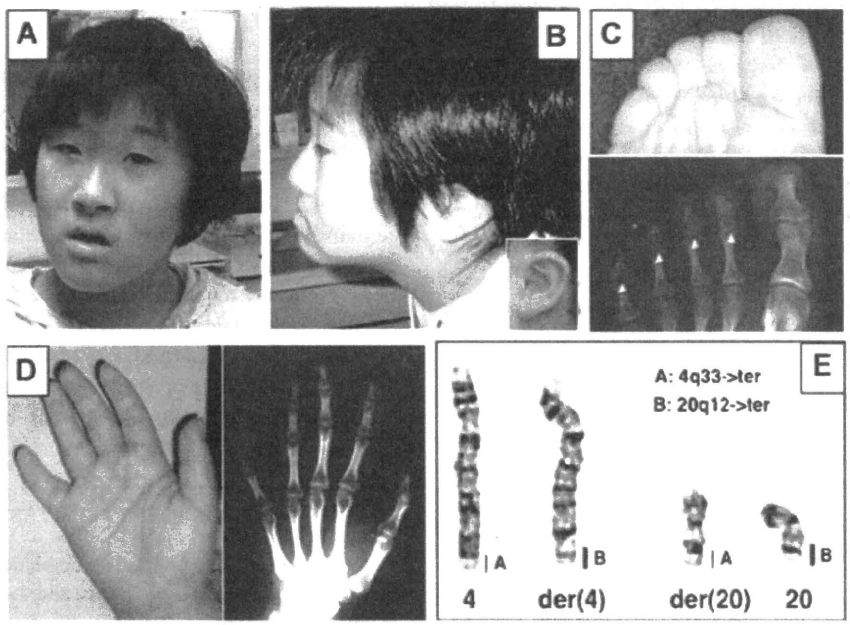

FIG. 1. Photographs of patient 1 and G-banded chromosomes 4 and 20. A: Photograph of patient 1 at 16 years of age. Frontal face showing a milder short philtrum and shallow supraorbital ridge. B: Lateral view. C: Feet display brachydactyly with shortness of the middle phalanx of toes. D: Hands display shortness of the fifth finger but X-rays show a normal bone structure. E: High resolution G-banding of prometaphase chromosomes of the translocation derivatives and their normal homologues. A reciprocal translocation t(4;20)(q33;q12) was identified.

147.2 cm (−1.9 SD), 63.4 kg (+1.5 SD), and 57.4 cm (+0.2 SD), respectively. She has minor anomalies of the face including a mildly short philtrum and shallow supraorbital ridge (Fig. 1A,B). In addition the patient has a number of gray hairs, hirsutism, hyperopia, astigmatism, deformity of the dental arch, and a high arched palate. The fifth finger on each hand appears short but X-rays of the hands show normal bone structure (Fig. 1D), indicating that the volume of interdigital soft tissue between the 4th and 5th fingers is increased. Her toes also appear short. X-rays of the feet showed brachydactyly of the middle phalanx of toes (Fig. 1C).

Patients 2 and 3 have CHARGE syndrome. A transition of 5458C>T resulting in a nonsense mutation (R1820X) and a 4-bp deletion (1412-5delTGAC) generating a frame-shift (471fs474X) in *CHD7* were identified, respectively. The clinical features of the patients are described in the supporting information text (the supporting information text may be found in the online version of this article).

Lymphoblastoid cell lines were established by the Institute for Developmental Research, Aichi Human Service Center, through Epstein–Barr virus transformation of peripheral blood samples obtained from the patients and controls with informed consent.

FISH Analysis

Chromosomal preparations were made from peripheral blood cultures using standard methods. FISH was performed according to the method described by Pinkel et al. [1988]. BACs used in this study were obtained from Invitrogen (Invitrogen, Carlsbad, CA). The digoxigenin-labeled BAC probes applied are shown in Figure 2. FISH slides were analyzed using a Microphoto-FXA with a triple-band pass filter (Nikon, Tokyo, Japan), a color chilled 3CCD camera (Hamamatsu Photonics, Hamamatsu), and PhotoShop (Adobe, San Jose, CA). FISH was performed on metaphase chromosomes of patient 1. BAC clones were chosen to span the regions around the breakpoints of 4q33 and 20q12 based on information from the NCBI human genome database. We also utilized BAC clones of CEP4 (VYSIS, Downers Grove, IL) as markers of the pericentromeric region of chromosome 4, a LSI ZNF217 clone (VYSIS) as a marker of 20q13.2, and whole chromosome paint FISH probes (WCP, VYSIS) specific for human chromosomes.

Southern Blot Analysis

Genomic DNA (10 μg) from patient 1 and three normal controls was digested with restriction enzymes, separated on a 0.9% agarose gel, and transferred by the alkaline method to a nylon membrane (Hybond-N+, GE Healthcare, Tokyo, Japan). The membrane was hybridized with three distinct [α-^{32}P]dCTP-labeled cDNA probes containing exons 19–30, exons 31–37, and a part of intron 27 of *CHD6*, respectively. A 590-bp probe at intron 27 containing a *Sac*I site was prepared by amplifying the control genomic DNA with

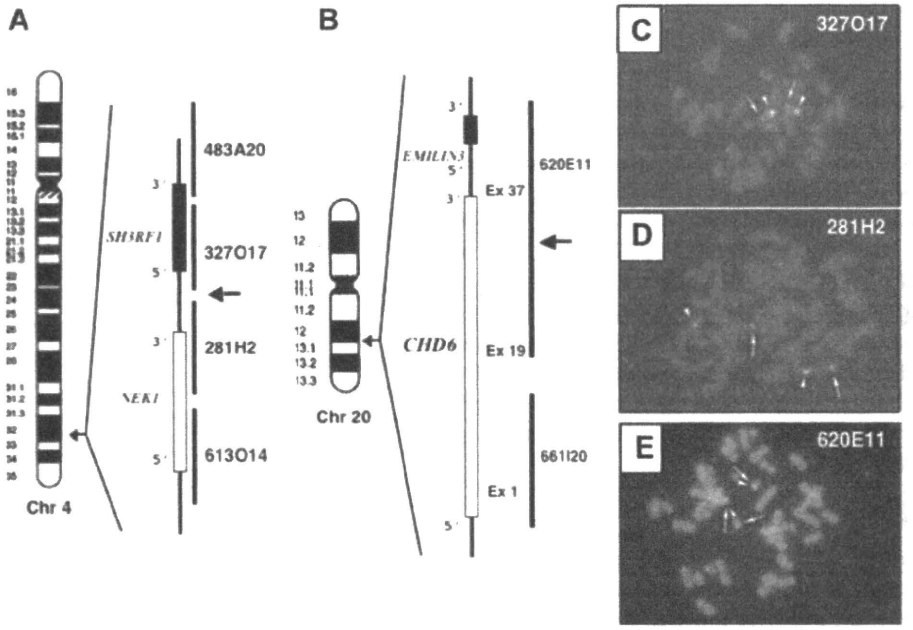

FIG. 2. FISH analysis of patient 1 to determine the breakpoint of 4q33 and 20q12. A: Schematic illustration of the genes and BAC clones at 4q33. Genes (*SH3RF1* and *NEK1*) and RP11-BAC clones (483A20, 327O17, 281H2, and 613O14) around the breakpoint are shown. The putative breakpoint is indicated by an arrow. B: Schematic illustration of the genes and BAC clones at 20q12. Genes (*EMILIN3* and *CHD6*) and RP4-BAC clones (620E11 and 661I20) around the breakpoint are shown. The putative breakpoint is indicated by an arrow. C: RP11-327O17 (red, indicated by arrows) hybridized with both the normal and der(4). D: RP11-281H2 (red, indicated by arrows) hybridized with both the normal chromosome 4 and der(20). E: RP4-620E11 (green) hybridized with the normal chromosome 20, der(20), and der(4). CEP4 (green) hybridized to the pericentromeric region of chromosome 4. LSI ZNF217 (red) hybridized to region 20q13.2 of der(4) and normal chromosome 20.

specific primers (sense: 5′-GCTGTGACATCTCAGGTGC-3′; antisense: 5′-CACAGCAAACTGATTGGTTAC-3′). Hybridization was performed with hybridization solution containing 5× standard saline citrate (SSC), 5× Denhardt's solution, and 0.5% SDS. The membranes were washed with 2× SSC, 0.1% SDS at 37°C for 20 min three times, and with 0.1× SSC containing 0.1% SDS at 55°C for 10 min three times, then exposed to X-ray film (FUJI RX-U, Fujifilm, Tokyo, Japan) at −80°C overnight.

DNA Sequencing

DNA fragments were isolated with a QIAEX II Gel Extraction Kit (Qiagen GmbH, Hamburg, Germany) and purified using polyethylene glycol (PEG 6000) precipitation. Sequencing of subcloned samples was performed on a SQ5500E DNA sequencer (Hitachi, Tokyo, Japan). Additional DNA fragments were sequenced directly with either the primers used for the PCR or specific inner primers [Yamada et al., 1992].

Characterization of the Breakpoint

FISH and Southern blot analysis revealed that the breakpoint fell within intron 27 of *CHD6*. This region contains the ~2.4 kb *Eco*RI/*Sac*I fragment of 20q12. To amplify a DNA fragment containing the breakpoint of der(20), one sense primer (a) was designed on the centromeric side of the breakpoint of 20q12 and five antisense primers (b1–5) on the telomeric side of the *Sac*I site of 4q33-ter, based on information in the NCBI database. The DNA fragment (~6 kb) containing the breakpoint was amplified with a primer pair a–b1. The sequences of the primers were as follows: sense (a): 5′-ACCAATCTACTAAACGGTTGCC-3′), antisense (b1): 5′-GGTACCTTGAGGCAAGGGTCA-3′. The breakpoint was determined by sequencing the 348-bp fragment amplified with inner primers 20S and 4A. The breakpoint of der(4) was determined by sequencing a 353-bp DNA fragment amplified with primers 4S and 20A. The sequences of these primers were as follows: 4S: 5′-TCATAACCTAGTGCACAACCT-3′, 4A: 5′-CCAAATTCTACAATATATCTGGC-3′, 20S: 5′-TGTGTGTGGTTTTAGCATGC-3′, and 20A: 5′-AGCTCATATGAAGAGGCCAG-3′. PCR was performed using AmpliTaq-Gold (Applied Biosystems, Foster City, CA), in a total volume of 20 µl. Reaction mixtures containing 100 ng of genomic DNA and 0.3 µM of each primer were preheated at 94°C for 10 min, and 36 cycles of PCR were performed. Each cycle consisted of 30 sec denaturation at 94°C, 30 sec annealing at 58°C, and 30 sec extension at 72°C.

Construction of Expression Vectors

To generate RNA interference constructs specific for *CHD6* or *CHD7*, the forward and reverse strands of oligos containing the 19-nt sequence of targeted genes were annealed and subcloned into the siRNA-expressing pSUPER vector (OligoEngine, Seatle, WA) (pSUPER-siCHD6, pSUPER-siCHD7). We chose expression vectors to decrease *CHD6* or *CHD7* expression to less than 50% that of mock (pSUPER) transfected cells.

Northern Blot Analysis

A human multiple-tissue Northern blot (Clontech Laboratories, Inc. Mountain View, CA) was hybridized in accordance with the manufacturer's directions with a 1,221-bp fragment containing exons 34–37 of *CHD6* cDNA as a probe. Next, total RNA was extracted from cultured lymphoblastoid cells of patient 1 and three normal controls with TRIzol Reagent (Invitrogen) and aliquots (10 µg) were electrophoresed through a 0.9% formaldehyde/agarose gel and transferred to a Hybond N+ membrane. The filter was hybridized with [α-^{32}P]dCTP-labeled 5′- and 3′-probes of *CHD6* cDNA or *TUBA1B* (α-tubulin) cDNA. After hybridization, the filter was washed to a final stringency of 0.1× SSC, 0.1% SDS at 60°C for 20 min. Autoradiography was accomplished using an intensifying screen. The *CHD6* cDNA fragment (from start codon ATG to *Bam*HI site, 1,020 bp) was used as 5′-probe. The 3′-DNA probe of *CHD6* (nt 7291–8341, 1,051 bp) was generated by amplification of genomic DNA with specific primers (sense: 5′-AGTTCCTGGCTTTGGGGCA-3′, antisense: 5′-TAAATGGTCGACGTTCTAATTGGTGTCGTTGT-3′). The *TUBA1B* cDNA probe was similarly generated by amplification of cDNA with specific primers (sense: 5′-ATCAAAACCAAGCGCAGCATC-3′, antisense: 5′-GGATAATTAGTATTCCTCTCCTT-3′). Amplified DNA probes were subcloned into pGEM-T Easy vectors, and their sequences were confirmed.

RT-PCR Analysis of CHD6, SH3RF1, NEK1, and ACTB mRNA

Total RNA was isolated from cultured lymphoblastoid cells of patient 1 and three normal controls with TRIzol Reagent and first-strand cDNAs were synthesized by reverse transcription of 4.5 µg of total RNA using First-Strand cDNA Synthesis Kit (GE Healthcare). The steady-state levels of *CHD6*, *SH3RF1*, and *NEK1* mRNA were analyzed by RT-PCR relative to β-actin (*ACTB*) as a control. Primer pairs were designed to amplify a 200-bp fragment from the last two exons of each gene. Aliquots (equivalent to 0.1 µg) of total RNA of first-strand cDNA were amplified by PCR in a total volume of 20 µl, each containing 0.3 µM of the primer pair for the target gene, 30 µM of each dNTP, 2.5 mM $MgCl_2$, 10 mM Tris–HCl (pH 8.3), 50 mM KCl, 1 U of AmpliTaq-Gold, and 0.2 µl of [α-^{32}P]dCTP (80 kBq: 111 TBq/mmol). PCR samples were preheated at 94°C for 10 min, and from 16 to 26 cycles were performed. Each cycle consisted of 30 sec denaturation at 94°C, 30 sec annealing at 58°C, and 30 sec extension at 72°C. PCR products were separated on 8% polyacrylamide gels and quantification of radioactivity was performed with a BAS 1800 image analyzer (FUJIFILM). Steady-state levels of *Chd6* mRNA of mouse cerebral cortex at various ages (E15.5, P0, P1, P2, P4, P7, P14, and P28) were analyzed using the same procedure.

Preparation of Antibodies

To prepare antibodies specific for the N-terminal (amino acids 1–120) and C-terminal (amino acids 2,596–2,715) regions of CHD6 and the C-terminal (amino acids 2,898–2,997) region of CHD7, GST fusion proteins were expressed in *E. coli* using pGEX6P-1 vectors (GE Healthcare). Lysates of *E. coli* were loaded onto a Glutathione Sepharose 4B (GE Healthcare) column. The column was washed with 20 column volumes of buffer 1 (20 mM Tris/HCl, pH 7.5, and 150 mM NaCl), 20 column volumes of buffer

2 (20 mM Tris/HCl, pH 7.5, and 500 mM NaCl), and finally equilibrated with buffer 3 (50 mM Tris/HCl, pH 7.0, 150 mM NaCl, 1 mM EDTA, and 1 mM DTT). GST fusion proteins were cleaved overnight with PreScission protease (GE Healthcare) in columns at 4°C, and CHD6 or CHD7 antigen proteins were eluted from Glutathione Sepharose 4B columns with buffer 1. Elution proteins were further purified with a gel filtration column (Sephadex G-75, GE Healthcare) equilibrated with buffer 1 and fractions containing CHD6 or CHD7 antigen proteins were collected. The purities of antigen proteins were confirmed by SDS–PAGE. Rabbit polyclonal antibodies specific for CHD6 or CHD7 antigen proteins were generated and affinity purified using a CNBr-activated Sepharose 4B (GE Healthcare) column conjugated with CHD6 or CHD7 antigen proteins. For immunohistochemistry, rabbit polyclonal antibodies were further purified using a CNBr-activated Sepharose 4B column conjugated with the C-terminal 31 amino acids of CHD6 (TKGDNPNSHPEPAPSCEREPSGDENCAEPSA) or CHD7 (CGSSEEKAADKAEGGPFKDGETLEGSDAEES), respectively. The following antibodies were also used for immunofluorescence staining or Western blotting: monoclonal mouse anti-α-tubulin antibody (Sigma–Aldrich, St. Louis, MO); monoclonal mouse anti-γ-tubulin antibody (Sigma–Aldrich); rabbit polyclonal anti-α-tubulin antibody (Sigma–Aldrich).

Western Blotting

Western blotting was performed with antibodies against CHD6, CHD7, and α-tubulin. CHD6- or CHD7-knockdown or mock transfected control HeLa cells were washed twice with PBS, extracted with 1% SDS and sonicated with SOMIFIER 250 (BRANSON, Danbury, CT). For analysis of CHD6 and CHD7, samples containing 30 μg protein were run on 6% SDS–PAGE, and for α-tubulin analysis, 0.5 μg aliquots of solubilized proteins were run on a 10% SDS–PAGE. Samples were then transferred to PVDF membranes (Immobilon-P, Millipore, Billerica, MA), and incubated with antibodies at 4°C overnight. After transfer, membranes were washed and incubated with a 1:20,000 dilution of anti-rabbit immunoglobulin horseradish peroxidase-conjugated antibody (Promega, Madison, WI) or a 1:6,000 dilution of anti-mouse immunoglobulin horseradish peroxidase-conjugated antibody (Medical & Biological Laboratories, Nagoya, Japan) and visualized with an enhanced chemiluminescence Western blotting detection system (GE Healthcare).

Metaphase Analysis of CHD6- or CHD7-Knockdown HeLa Cells

A 1.6 μg aliquot of pSUPER-siCHD6, pSUPER-siCHD7, control vector (pSUPER), or siRNA (100 nM of non-target and for *CHD6*) (Dharmacon, Chicago, IL) was transfected into HeLa cells in 12-well plates using Lipofectamine 2000 Reagent (Invitrogen). Twenty-four hours after transfection, cells were harvested and replated on poly-L-lysine-coated coverslips. They were then cultured for an additional 36 hr at 37°C in a humidified atmosphere of 5% CO_2, fixed with 2% paraformaldehyde in PBS at room temperature for 20 min, and rinsed with PBS three times. Cells on coverslips were subjected to 0.5% Triton X-100 in PBS for 5 min and blocked with PBS containing 3% BSA for 30 min. For double immunolabeling of cells, rabbit polyclonal anti-α-tubulin and mouse anti-γ-tubulin antibodies, or mouse anti-γ-tubulin and rabbit polyclonal anti-pericentrin antibodies were applied. Anti-mouse IgG conjugated with Alexa Fluor 488 and anti-rabbit IgG conjugated with Alexa Fluor 594 were used as secondary antibodies (Molecular probes, Eugene, OR). After counterstaining with DAPI, coverslips with fixed cells were mounted on glass slides for fluorescence microscopy. U-MNIBA, U-MWIG, and U-MWU were used to detect DAPI, Alexa Fluor 488, and Alexa Fluor 594, respectively. Misaligned chromosomes were classified as described in Toyoda and Yanagida [2006]. Cells with all chromosomes aligned on the equatorial plane (metaphase plate) were described as "aligned," those with one or two chromosomes separated and misaligned from the metaphase plate as "few," and examples with more than three misaligned chromosomes as "plentiful" (Fig. 6B). We distinguished cells with severely misaligned chromosomes at metaphase from cells at prometaphase applying the following criteria: (1) Chromosomes aligned on the metaphase plate are distinctly condensed and shortened compared with chromosomes at prometaphase; (2) centrosomes are located distantly from and on both side of the metaphase plate.

RESULTS

Identification of Translocation Breakpoints

A reciprocal translocation t(4;20)(q33;q12) was identified in patient 1 by G-banding (Fig. 1E). The finding that the parents are healthy with normal karyotypes indicated the translocation to be a de novo event (data not shown). FISH analysis with whole chromosome painting probes (WCP) confirmed the translocation of t(4;20)(q33;q12) as the sole chromosomal abnormality (data not shown). To determine the translocation breakpoints, we first narrowed the regions around the breakpoints by FISH analysis with locus-specific BAC clones. We then determined that the breakpoint of 4q33 was located between two BAC clones RP11-327O17 and RP11-281H2 (Fig. 2C,D) and the breakpoint of 20q12 was within RP4-620E11 (Fig. 2E) (GenBank accession numbers are as follows, RP11-327O17; AC096741, RP11-281H2; AC116621, RP4-620E11; AC031667). The breakpoint of 4q33 localized to a region between two genes, *SH3RF1* and *NEK1*, while the breakpoint of 20q12 potentially localized to *CHD6* as the RP4-620E11 BAC clone contains part of *CHD6* (exons 19–37) (Fig. 2). To determine if the *CHD6* locus was disrupted by this translocation, we analyzed *Eco*RI-digested genomic DNA by Southern blotting with probes comprising two parts of the *CHD6* cDNA (exons 19–30 and 31–37). The patient's DNA showed patterns identical to those of controls (data not shown). As the *CHD6* cDNA probes could not detect parts of intron 27 (3.1 and 3.6 kb of *Eco*RI fragments) (Fig. 3A), we performed additional Southern blot analysis of *Sac*I or *Eco*RI-digested genomic DNA using a 590-bp intron probe containing a *Sac*I site (Fig. 3A). In genomic DNA from patient 1, the intensity of the 3.5-kb band of *Sac*I-digested DNA was decreased and an additional ~7-kb band was present. In contrast, the banding pattern was identical for the patient and control DNA when digested with *Eco*RI (Fig. 3B). Thus, the breakpoint of 20q12 was determined to be located in the 2.4 kb *Eco*RI/*Sac*I fragment region of intron 27 (Fig. 3A).

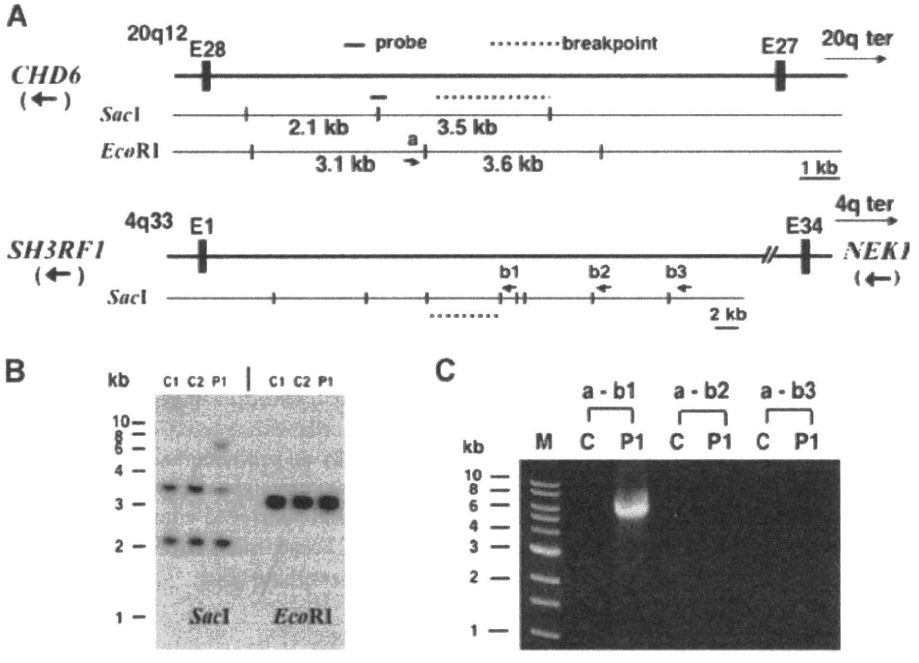

FIG. 3. Amplification of genomic DNA containing a translocation breakpoint on der(20). A: Schematic diagram of part of the genomic structures of *CHD6* at 20q12 and of *SH3RF1* at 4q33. The upper panel shows exon 27, intron 27, and exon 28 of *CHD6* and the restriction enzyme sites of *SacI* and *EcoRI*. The lower panel shows exon 1 and the 5′-flanking region of *SH3RF1* and *SacI* restriction sites. The probe used for Southern blot analysis is shown as a black line and the putative breakpoint region is indicated as a dotted line. Primers used for PCR analysis are shown as arrows (a, b1–3). B: Southern blot analysis of the controls' DNA and the patient's DNA. Genomic DNA (10 μg) of two controls and patient 1 was digested with *SacI* or *EcoRI*, electrophoresed through a 0.9% agarose gel, transferred to a Hybond N+ membrane, and hybridized with a [^{32}P]-labeled intron 27 probe. C1 and C2, controls; P1, patient 1. C: Genomic DNA from patient 1 and a normal control were amplified using specific primer pairs (a–b1, a–b2, a–b3) and electrophoresed through a 1.0% agarose gel. C, control; P1, patient 1; M, 1 kb DNA ladder.

The patient's derivative chromosome 20 (der(20)) lacks the distal part of the long arm of chromosome 20 (20q12 → ter). Instead, the telomeric region of chromosome 4 (4q33 → ter) is translocated to der(20). Therefore, the breakpoint of der(20) is near the 5′-region of *SH3RF1* (Figs. 2A and 3A). To determine the sequence at the breakpoint on der(20), one sense primer (a) was chosen near the *Eco*RI site at the centromeric side of the breakpoint on chromosome 20, and five antisense primers (b1–b5) were chosen near the *Sac*I site on the telomeric side of the breakpoint at chromosome 4. One of the primer pairs, a–b1, successfully amplified an ~6-kb band (Fig. 3C). The fragment was subcloned into the *Eco*RI and *Sac*I sites of pBluescript KS(+) and sequenced with internal primers. A 348-bp DNA fragment containing the breakpoint of 20q12 was amplified exclusively from the genomic DNA of patient 1 with one primer pair (20S-4A) (Fig. 4B2). Sequencing of the fragment revealed that in patient 1, the nucleotide sequence which follows *CHD6* intron 27 sequence (5′-. . .GCAAAT-3′) differs from the expected sequence (5′-CATAAA. . .-3′) (Fig. 4C1 and 2). Rather, the new sequence (5′-ACTCAA. . .-3′) was identical to the 5′-flanking region of *SH3RF1* at 4q33 (Fig. 4C3). Next, we chose one primer on the centromeric side (4S) of the determined breakpoint for chromosome 4 and another on the telomeric side of intron 27 (20A) of *CHD6* in order to amplify the patient and control genomic DNA. Only a DNA fragment (353 bp) containing the breakpoints present in the patient's genomic DNA was amplified (4S-20A) (Fig. 4B4). Sequencing of this fragment revealed a different nucleotide sequence (5′-ATTTATGTGTT. . .-3′) after the 5′-flanking region of *SH3RF1* (5′-. . .TTGCCC-3′) (Fig. 4C4). An NCBI BLAST search identified the new nucleotide sequence (5′-ATGTGTT. . .-3′) as that of intron 27 of *CHD6* with the addition of four nucleotides (5′-ATTT-3′) (Fig. 4C1). The sequence near the breakpoint on der(4) contained an additional ATTT. A longer DNA fragment amplified from control DNA using the primer pair 4S-20A proved to be an artifact following direct sequencing. There is a 5-bp deletion (CATAA)/4-bp insertion (ATTT) on der(4) and a 3-bp deletion (GCC) on der(20) at these breakpoints, respectively. Thus, patient 1 has a balanced translocation t(4;20)(q33;q12), with the breakpoint of 20q12 in intron 27 of *CHD6* and that of 4q33 ~16.0 kb upstream of *SH3RF1* and 106.2 kb downstream of *NEK1*.

Steady-State Levels of CHD6 mRNA Are Decreased in Lymphoblastoid Cells of Patient 1

We first performed quantitative RT-PCR analyses of lymphoblastoid cell lines using gene-specific primer pairs for 18–22 PCR cycles,

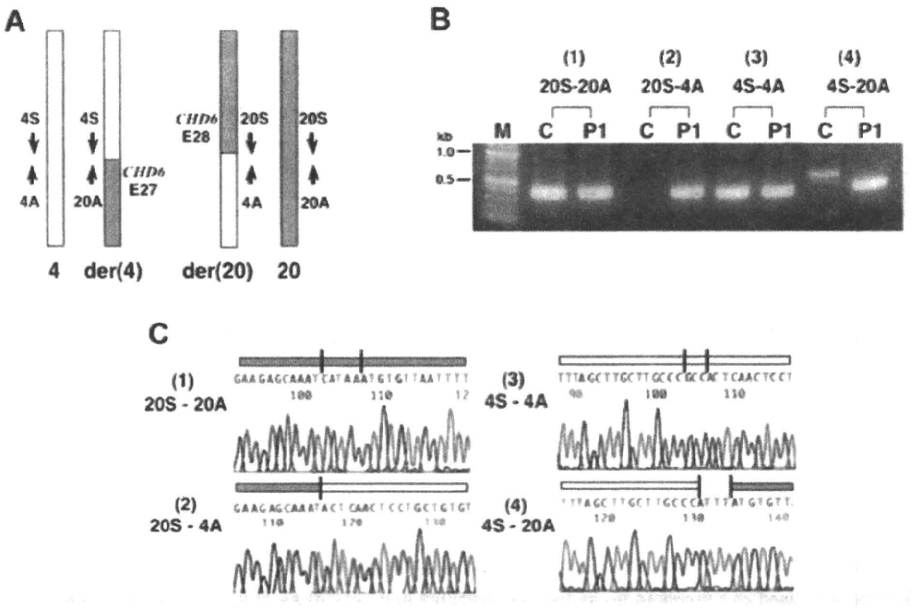

FIG. 4. Nucleotide sequences of the breakpoints. A: Schematic representation of normal and derivative chromosomes 4 and 20 of patient 1. Primer pairs 4S-20A and 20S-4A were designed for amplification of DNA fragments including breakpoints on der(4) and der(20), respectively. Primer pairs 4S-4A and 20S-20A amplified DNA fragments containing the sequences around the breakpoints on chromosomes 4 and 20, respectively. The open box represents all and part of chromosome 4. The closed box represents all and part of chromosome 20. der(4) contains exons 1–27 of *CHD6* and der(20) contains exons 28–37 of *CHD6*. B: PCR amplification of DNA fragments from normal and derivative chromosomes with specific primer pairs. C, control; P1, patient 1; M, 100 bp DNA ladder. C: Sequence chromatograms of the DNA fragments amplified with the specific primer pairs (1) 20S-20A, (2) 20S-4A, (3) 4S-4A, and (4) 4S-20A.

which showed a linear correlation of products with the number of cycles performed [Wakamatsu et al., 1992]. This analysis showed the steady-state level of the patient's *CHD6* mRNA to be decreased to ~50% of those of three normal controls while the steady-state levels of *SH3RF1* and *NEK1* mRNA were as same as in controls (Fig. 5A). We next confirmed decreased expression of the patient's *CHD6* mRNA by Northern blot analysis using a part of the 5′- or 3′-region of *CHD6* cDNA as a probe. Steady-state levels of the patient's *CHD6* mRNA was decreased to ~50% but of similar size (~10 kb) to those of controls (Fig. 5B). No other size of *CHD6* mRNA was detected in the patient's lymphoblastoid cells (Fig. 5B).

Tissue Distribution and Developmental Expression of CHD6 and Its Mouse Ortholog

Northern blot analysis using a *CHD6* probe (exons 34–37, 1,221 bp) on mRNA samples from 12 different tissues of human adults revealed expression of a 10.4-kb mRNA in brain, heart, skeletal muscle, kidney, small intestine, placenta, lung, and peripheral blood leukocytes (Fig. 5C). Expression was most pronounced in skeletal muscle and barely detectable in colon, thymus, spleen, and liver. In mouse cerebral cortex, orthologous *Chd6* mRNA expression was detected at E15.5 and increased gradually after birth (P0-28) (Fig. 5D).

Knockdown of CHD6 or CHD7 Results in Impairment of Chromosome Alignment

As CHD proteins are nucleosome-remodeling factors, we hypothesized that cells from patients with loss of function mutations in CHD subfamily III genes (i.e., *CHD6* and *CHD7*) may have defects in chromosome dynamics during the cell cycle. To study this hypothesis, we knocked down CHD6 or CHD7 expression in HeLa cells by transfection of siRNA expression vectors (Fig. 6A), and analyzed chromosome dynamics of metaphase cells. The frequency misaligned chromosomes on the metaphase plate ("plentiful" in Table I) was increased by at least twofold in CHD6 or CHD7 knockdown HeLa cells than in control cells (no treatment or pSUPER transfection) (Table I and Fig. 6B).

Patients With CHD6 or CHD7 Mutations Exhibit Aneuploidy

Chromosomal preparations were made from lymphoblastoid cells using standard method. Analysis of 300 metaphase lymphoblastoid cells from patients 1–3 and three normal controls revealed that all patients have a rate of abnormal chromosome number of >15.6%. This frequency of aneuploidy is more than twice the abnormal chromosome rate in control cells (<7.7%, Table II).

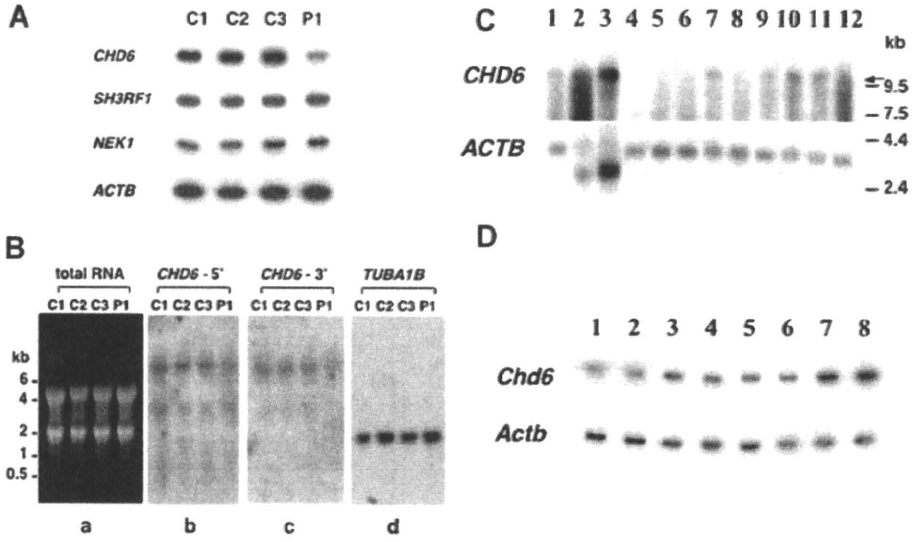

FIG. 5. CHD6 expression profiles. A: RT-PCR analysis of *CHD6*, *SH3RF1*, and *NEK1* mRNA in patient 1 and normal lymphoblastoid cells using RT-PCR. The amount of *ACTB* mRNA was used as a standard to estimate the amounts of other mRNAs. PCR cycles for each gene were as follows: *CHD6*, 22; *SH3RF1*, 24; *NEK1*, 26; *ACTB*, 16. C1-3, normal controls; P1, patient 1. B: Northern blot analyses of lymphoblastoid cells from three normal controls and patient 1. Total RNAs (10 μg) of lymphoblastoid cells from three controls and patient 1 were separated on a 0.9% formaldehyde/agarose gel, stained using ethidium bromide (a), transferred to Hybond N+ membrane, and hybridized using an [α-^{32}P]-labeled 5′-*CHD6* probe (b). After removal of the probe, the same membrane was hybridized with [α-^{32}P]-labeled 3′-*CHD6* probes (c), and *TUBA1B* (d). C1-3, normal controls; P1, patient 1. C: Expression patterns of *CHD6*. Autoradiographs of Northern blots hybridized with a 1.2-kb *CHD6* cDNA (exons 34–37) and a 2.0-kb human *ACTB* (β-actin) cDNA as a standard. Lane 1, brain; lane 2, heart; lane 3, skeletal muscle; lane 4, colon; lane 5, thymus; lane 6, spleen; lane 7, kidney; lane 8, liver; lane 9, small intestine; lane 10, placenta; lane 11, lung; and lane 12, peripheral blood leukocyte. *CHD6* mRNA was ~10.4 kb in size, and is indicated by an arrow. D: Expression patterns of *Chd6* in mouse cerebral cortex. Total RNA was extracted from mouse cerebral cortex at various ages and steady-state levels of *Chd6* mRNA and *Actb* mRNA were analyzed by RT-PCR. Lane 1, E15.5; lane 2, P0; lane 3, P1; lane 4, P2; lane 5, P4; lane 6, P7; lane 7, P14; lane 8, P28.

DISCUSSION

In this study, we report a patient (patient 1) with a balanced translocation t(4;20)(q33;q12) presenting with severe mental retardation, brachydactyly of the toes and minor anomalies of the face. We localized the translocation breakpoint to intron 27 of *CHD6*, and Northern blot analysis using 5′- and 3′-probes showed the steady-state levels of *CHD6* mRNA in lymphoblastoid cells of the patient to be decreased by ~50% without any alteration in transcript size. Thus, haploinsufficiency of *CHD6* is most likely responsible for the clinical features of patient 1. We searched reported cases of patients harboring aberrant chromosome structures (deletions or translocations) around *CHD6* locus (20q12). Recently, a female harboring a de novo translocation t(18;20)(q21.1;q11.2) with moderate mental retardation and minor facial anomalies was reported [Kalscheuer et al., 2008]. In this case, the breakpoint of 18q21.1 was located in intron 3 of *TCF4*, whereas the breakpoint of 20q11.2 was located in intron 1 (exon 1 contains only the 5′-untranslated region) of *CHD6*. Moreover, fusion transcripts of the genes were identified. Thus, this is not a case of *CHD6* haploinsufficiency. A female with interstitial microdeletion of 20q11.22-q12 has also been reported, but *CHD6* was not included in the deletion area [Callier et al., 2006]. Taken together, patient 1 is the first reported case of symptoms resulting from *CHD6* haploinsufficiency. Identification and characterization of similar cases with breakpoints, deletions, or mutations involving *CHD6* is necessary to clarify the clinical features of *CHD6* haploinsufficiency.

CHD6 belongs to the largest subfamily, subfamily III (CHD6–9), of the CHD family of proteins (CHD1–9), which were recently found to possess ATP-dependent chromosome-remodeling activity and an ability to regulate transcription through mobilization of chromatin structures [Nioi et al., 2005; Shur et al., 2006; Yuan et al., 2007; Thompson et al., 2008]. These functions are associated with chromo-domains and an SNF2-related helicase/ATPase domain, both common to all CHD family proteins (CHD1–9). CHD6–9 are very large proteins (>300 kDa) containing other domains on the N-terminal and C-terminal sides of these common domains. Moreover, CHD6 and CHD7 have very similar amino acid sequence and the C-terminal 610 amino acids of CHD6 show 35% homology with the C-terminal 670 amino acids of CHD7. To investigate the cellular mechanism of disease in patient 1 resulting from CHD6 haploinsufficiency, we reduced CHD6 or CHD7 function by RNA interference in HeLa cells and examined chromosome dynamics during the cell cycle. Our studies demonstrated that the frequencies of cells with extensively misaligned chromosomes ("plentiful" in Table I) were increased at least twofold upon CHD6- or CHD7-knockdown. During mitosis, duplicated sister chromatids condense gradually, align to the metaphase plate, and subsequently segregate to oppos-

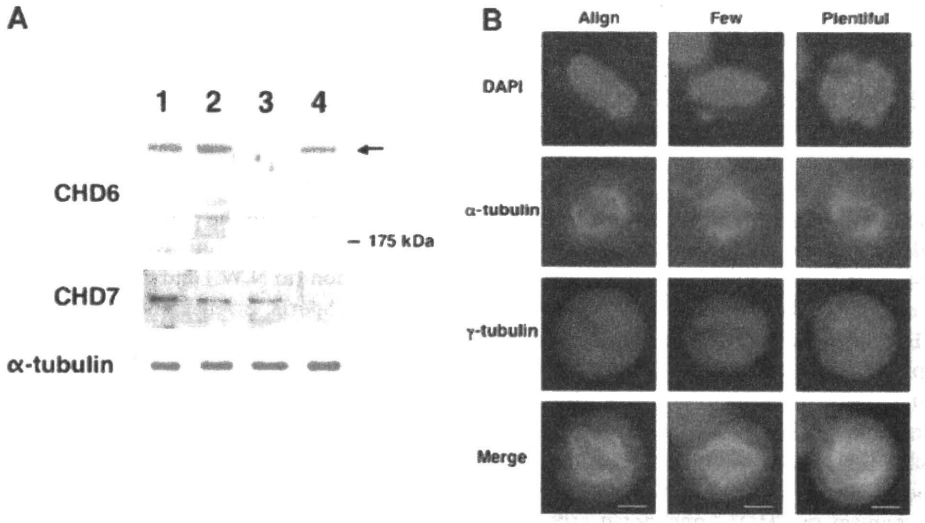

FIG. 6. Effects of RNAi-mediated knockdown of CHD6 or CHD7 on chromosome alignment in metaphase HeLa cells. A: RNAi-mediated knockdown of CHD6 or CHD7. pSUPER-siCHD6, pSUPER-siCHD7, or pSUPER (control vector) were transfected into HeLa cells. At 60 hr after transfection, cells were harvested and proteins were extracted and analyzed by Western blot analyses using antibodies specific for α-tubulin, CHD6 and CHD7. Lane 1, non-trasfected HeLa cells; lane2, pSUPER; lane 3, pSUPER-siCHD6; lane 4, pSUPER-siCHD7. The arrow indicates signals for CHD6, and the protein-molecular marker (175 kDa) is shown on the panel of CHD6. B: Misaligned chromosomes in CHD6- or CHD7-knockdown HeLa cells. pSUPER-siCHD6, pSUPER-siCHD7, or pSUPER were transfected into HeLa cells. At 60 hr after transfection, cells were fixed and stained with anti-α-tubulin (red) and anti-γ-tubulin antibodies (green). Chromosomes were stained with DAPI (blue). Images represent cells containing aligned chromosomes (aligned, left), one or two misaligned chromosomes (few, middle), and three or more misaligned chromosomes (plentiful, right), respectively. Scale bar indicates 10 μm.

TABLE I. Effects of RNAi-Mediated Knockdown of CHD6 or CHD7 on Chromosome Alignment in Metaphase HeLa Cells

Alignment	Control % (n)	Vector (pSUPER) % (n)	CHD6 (pSUPER) % (n)	CHD7 (pSUPER) % (n)	siRNA (control) % (n)	siRNA (CHD6) % (n)
Aligned	88.0 (938)	86.6 (428)	76.1 (290)	77.5 (238)	87.0 (559)	76.8 (464)
Few	5.4 (57)	5.7 (28)	6.8 (26)	4.9 (15)	6.2 (40)	7.1 (43)
Plentiful	6.6 (70)	7.7 (38)	**17.1** (65)	**17.6** (54)	6.8 (44)	**16.1** (97)
Total	100 (1,065)	100 (494)	100 (381)	100 (307)	100 (643)	100 (604)

Bold typing means the significance of group differences (p-value of <0.05) analyzed with one-way analysis of variance followed by Bonferroni correction for multiple comparisons.

ing spindle poles. Precise alignment of the chromosomes at the metaphase plate is crucially important because misaligned chromosomes may cause mitotic arrest and/or premature segregation which can lead to aneuploidy and/or cell death. Toyoda and Yanagida [2006] reported that cells displaying extensively misaligned chromosomes are remarkably increased in HeLa cells knocked down for hRad21, a component of the cohesin complex. The authors concluded that this is the earliest phenotype in cells harboring mitotic delay. Thus, the increase in the amount of extensively misaligned chromosomes in CHD6- or CHD7-knock-

TABLE II. Chromosome Numbers of Lymphoblastoid Cells From Patients 1–3 and Normal Controls

2n	41	42	43	44	45	46	47	48	49	50	51	52	53	54	55	56	57	Aneuploidy (%)
Control 1	1		1	4	15	277	1	1										7.7
Control 2				4	10	283	2	1										5.7
Control 3			1	8	11	278	1		1									7.3
P1 (CHD6)		5	6	14	19	245	7	1		1	1					1		18.3
P2 (CHD7)	1	2	5	9	20	251	7	2	1				1				1	16.3
P3 (CHD7)			3	9	24	253	10	1										15.6

down HeLa cells suggests that these two proteins also play important roles in chromosome alignment at metaphase.

A recent study demonstrated that other CHD family proteins, specifically subfamily II members (CHD3 and CHD4), also play important roles in chromosome dynamics. CHD3 predominantly co-localized with pericentrin (a component of pericentriolar materials, an electron-dense matrix which surrounds the centrosome) at metaphase and CHD3-knockdown HeLa cells exhibited dissociation of pericentrin from centrosomes, which caused metaphase delay, mitotic failure, and cytokinesis defects. Additionally, CHD4 negatively regulates the amount of pericentrin at the centrosome [Sillibourne et al., 2007]. Thus, CHD subfamily II and III proteins are associated with chromosome alignment at metaphase. Since CHD6 and CHD7 are diffusely localized throughout the cell at metaphase (supporting information Fig. 1, supporting information Fig. 1 may be found in the online version of this article), the cellular mechanism resulting in misaligned chromosomes in CHD6- or CHD7-knockdown cells likely differs from the mechanism in CHD3-knockdown cells. Further study is required to clarify the role of CHD6 and CHD7 in chromosome alignment in more detail.

It is important to analyze chromosome alignment in patients' cells to evaluating the pathogenesis of disease. We used lymphoblastoid cells for this purpose. Because lymphoblastoid cells are suspension cells, it is difficult to analyze chromosome alignment directly. Instead, we examined aneuploidy (an incorrect number of chromosomes) of the lymphoblastoid cells. The observed elevated frequency of aneuploidy is suggestive that the patients have abnormal chromosome alignment as a result of CHD6 or CHD7 mutation. In humans, aneuploidy is the major cause of miscarriages and mental retardation [Pai et al., 2003]. A relatively minor two- to threefold increase of aneuploidy might account, at least in part, for mental retardation of patients 1–3, which is more mild than cancer or prenatal death.

CHD7 is the only gene known to be causal for CHARGE syndrome. Curiously, the clinical features of patient 1 are quite different from those of the established CHARGE syndrome caused by *CHD7* mutation, save for mental retardation. Using chromatin immunoprecipitation on tiled microarrays (ChIP-chip), CHD7 was localized to discrete locations along chromatin specific to each cell type and ES cell differentiation state [Schnetz et al., 2009]. Thus, differences in target genes regulated by the chromatin-remodeling activity of CHD6 or CHD7 may explain the range of clinical features.

Kulkarni et al. [2008] reported a female patient with a de novo translocation in *CHD2* presenting scoliosis, hirsutism, learning problems, and developmental delay, syndactyly of the toes should also be noted. Brachydactyly is defined as disproportionately short fingers and toes, and forms part of the group of limb malformations [Temtamy and McKusick, 1978]. Our patient showed brachydactyly of the middle phalanx of toes. Nearly two-thirds (19/31) of individuals suffering from CHARGE syndrome have scoliosis [Doyle and Blake 2005]. Moreover, CHD9 regulates transcription during differentiation of osteogenic cells [Shur and Benayahu, 2005; Shur et al., 2006]. Thus, mutations of CHD family genes are candidate causal factors in patients with abnormal development of bones.

In summary, we have reported the first patient with a mutation identified in *CHD6* which is causative for mental retardation with minor anomalies. We also showed that loss of function mutations of *CHD6* or *CHD7* are associated with impairment of chromatin/chromosome assembly during mitosis.

ACKNOWLEDGMENTS

We are grateful to the patients who participated in this study and their families. This study was supported by the Uehara Memorial Foundation (to N.W.) and grants from the Ministry of Education, Culture, Sports, Science and Technology of Japan (to K.Y. and N.W.).

REFERENCES

Callier P, Faivre L, Marle N, Thauvin-Robinet C, Sanlaville D, Gosset P, Pieur M, Labenne M, Huet F, Mugneret F. 2006. Major feeding difficulties in the first reported case of interstitial 20q11.22-q12 microdeletion and molecular cytogenetic characterization. Am J Med Genet Part A 140A:1859–1863.

Doyle C, Blake K. 2005. Scoliosis in CHARGE: A prospective survey and two case reports. Am J Med Genet Part A 133A:340–343.

Ishihara K, Oshimura M, Nakao M. 2006. CTCF-dependent chromatin insulator is linked to epigenetic remodeling. Mol Cell 23:733–742.

Kalscheuer VM, Feenstra I, Van Ravenswaaij-Arts CM, Smeets DF, Menzel C, Ullmann R, Musante L, Ropers HH. 2008. Disruption of the TCF4 gene in a girl with mental retardation but without the classical Pitt-Hopkins syndrome. Am J Med Genet Part A 146A:2053–2059.

Kulkarni S, Nagarajan P, Wall J, Donovan DJ, Donell RL, Ligon AH, Venkatachalam S, Quade BJ. 2008. Disruption of chromodomain helicase DNA binding protein 2 (CHD2) causes scoliosis. Am J Med Genet Part A 146A:1117–1127.

Lutz T, Stoger R, Nieto A. 2006. CHD6 is a DNA-dependent ATPase and localizes at nuclear sites of mRNA synthesis. FEBS Lett 580: 5851–5857.

Nioi P, Nguyen T, Sherratt PJ, Pickett CB. 2005. The carboxy-terminal Neh3 domain of Nrf2 is required for transcriptional activation. Mol Cell Biol 25:10895–10906.

Pai GS, Lewandowski RC, Borgaonkar DS. 2003. Handbook of chromosomal syndromes. New York: Wiley-Liss.

Pinkel D, Landegent J, Collins C, Fuscoe J, Segraves R, Lucas J, Gray J. 1988. Fluorescence in situ hybridization with human chromosome-specific libraries: Detection of trisomy 21 and translocations of chromosome 4. Proc Natl Acad Sci USA 85:9138–9142.

Schnetz MP, Bartels CF, Shastri K, Balasubramanian D, Zentner GE, Balaji R, Zhang X, Song L, Wang Z, LaFramboise T, Crawford GE, Scacheri PC. 2009. Genomic distribution of CHD7 on chromatin tracks H3K4 methylation patterns. Genome Res 19:590–601.

Schuster EF, Stoger R. 2002. CHD5 defines a new subfamily of chromodomain-SWI2/SNF2-like helicases. Mamm Genome 2:117–119.

Shur I, Benayahu D. 2005. Characterization and functional analysis of CReMM, a novel chromodomain helicase DNA-binding protein. J Mol Biol 352:646–655.

Shur I, Socher R, Benayahu D. 2006. In vivo association of CReMM/CHD9 with promoters in osteogenic cells. J Cell Physiol 207:374–378.

Sillibourne JE, Delaval B, Redick S, Sinha M, Doxsey SJ. 2007. Chromatin remodeling proteins interact with pericentrin to regulate centrosome integrity. Mol Biol Cell 9:3667–3680.

Stokes DG, Perry RP. 1995. DNA-binding and chromatin localization properties of CHD1. Mol Cell Biol 5:2745–2753.

Temtamy SA, McKusick VA. 1978. The genetics of hand malformations. New York: Alain R Liss, Inc. p. 619.

Thompson BA, Tremblay V, Lin G, Bochar DA. 2008. CHD8 is an ATP-dependent chromatin remodeling factor that regulates beta-catenin target genes. Mol Cell Biol 12:3894–3904.

Toyoda Y, Yanagida M. 2006. Coordinated requirements of human topo II and cohesin for metaphase centromere alignment under Mad2-dependent spindle checkpoint surveillance. Mol Biol Cell 17:2287–2302.

Vissers LE, van Ravenswaaij CM, Admiraal R, Hurst JA, de Vries BB, Janssen IM, van der Vliet WA, Huys EH, de Jong PJ, Hamel BC, Schoenmakers EFPM, Brunner HG, Veltman JA, van Kessel AG. 2004. Mutations in a new member of the chromodomain gene family cause CHARGE syndrome. Nat Genet 36:955–957.

Wakamatsu N, Kobayashi H, Miyatake T, Tsuji S. 1992. A novel exon mutation in the human beta-hexosaminidase beta subunit gene affects 3' splice site selection. J Biol Chem 267:2406–2413.

Woodage T, Basrai MA, Baxevanis AD, Hieter P, Collins FS. 1997. Characterization of the CHD family of proteins. Proc Natl Acad Sci USA 94:11472–11477.

Yamada Y, Goto H, Suzumori K, Adachi R, Ogasawara N. 1992. Molecular analysis of five independent Japanese mutant genes responsible for hypoxanthine guanine phosphoribosyltransferase (HPRT) deficiency. Hum Genet 90:379–384.

Yuan CC, Zhao X, Florens L, Swanson SK, Washburn MP, Hernandez N. 2007. CHD8 associates with human Staf and contributes to efficient U6 RNA polymerase III transcription. Mol Cell Biol 24: 8729–8738.